Heliyon 10 (2024) e38820

Contents lists available at ScienceDirect

Heliyon

journal homepage: www.cell.com/heliyon

Research article

Exploring the protective effect of silver *Croton tiglium* nano-extract against azoxymethane induced toxicity in female reproductive organs in rats

Wael Mahmoud Aboulthana [a,1], Abd El-Nasser A. Madboli [b,1], Amal Gouda Hussien [a], Mohamed Seif [c,*]

[a] *Biochemistry Department, Biotechnology Research Institute, National Research Centre, 33 El-Bohouth St. Dokki, 12622, Giza, Egypt*
[b] *Animal Reproduction and Artificial Insemination Department, Veterinary Research Institute, National Research Centre, 33 El-Buhouth St., Dokki, 12622, Giza, Egypt*
[c] *Food Toxicology and Contaminants Department, Food Industries and Nutrition Research Institute, National Research Centre, 33 El-bohouth St., Dokki, Giza, P.O. Box.12622, Egypt*

ARTICLE INFO

Keywords:
Anti-tumour
Azoxymethane
Croton tiglium
Food contaminants, Immunohistochemistry

ABSTRACT

Reproductive toxicity from food and environmental contaminants has greatly affected human life. Plants are a fundamental source of bioactive components for relieving the harmful effects of pollutants. Hydrazine metabolites pose health threats when they enter the food chain. *Croton tiglium* (*C. tiglium*) exhibits anti-inflammatory and anti-tumor properties. Silver nanoparticles enhance the chemical stability of *C. tiglium*. Reproductive toxicity of Azoxymethane (AOM) and anticancer effects of silver *C. tiglium* were evaluated. Thirty-six adult female rats were divided into six groups ($n = 6$) and treated with AOM with or without silver *C. tiglium* nano-extract as pre- and post-treatment. Sexual hormones and proteins were assessed under silver *C. tiglium* nano-extract and AOM. Histopathologically, AOM caused metaplastic myometrial endometriotic cysts and endometrial metaplasia. Silver *C. tiglium* in pre- and post-treated rats mitigated the carcinogenic effects of AOM. Immunohistochemically, AOM carcinogenicity was evident through moderate detection of the CK-7 tumor marker in the ovaries and uterus of the AOM-, simultaneous-, and post-treated groups. *C. tiglium* ameliorated this, with CK-7 slightly expressed in the pre-treated group. Furthermore, *C. tiglium* alleviated the negative impact on FSH, LH, and 17-β estradiol hormones. In conclusion, Silver *C. tiglium* nano-extract successfully prevented tumors in the ovaries and uterus of AOM-treated rats.

1. Introduction

Environmentally, hydrazine (N_2H_4) is one of the groups of strong reducing agents called hydro-nitrogen compounds produced at a rate of 45000 tons annually. Hydrazines are also synthesized chemically from dimethylamine, ammonia, sodium hypochlorite, or hydrogen peroxide. It is utilized in several synthetic pesticides, manufacturing of the foam rubber, and used in boilers as a corrosion

* Corresponding author. Food Toxicology and Contaminants Department, Food Industries and Nutrition Research Institute, National Research Centre, 33 El- Bohouth St., Dokki, Giza, P.O. Box.12622, Egypt.
E-mail address: seif.eg@gmail.com (M. Seif).
[1] These authors contributed equally.

https://doi.org/10.1016/j.heliyon.2024.e38820
Received 9 May 2024; Received in revised form 28 August 2024; Accepted 30 September 2024
Available online 5 October 2024

inhibitor. Recently, hydrazine and its derivatives were applied in the preparation of agricultural chemicals, which increased their hazards as food contaminants [1–3]. Hydrazine poses a threat to various components of the environment, possibly resulting in food contamination, which in turn causes harmful effects on human health and animal productivity [4–6]. Seizures, pulmonary injury, and death are the hazardous results due to exposure to the hydrazine derivatives even in in small amounts [7,8]. Besides, dermal exposure to the derivatives of hydrazine leads to erythema, dermatitis that is exaggerated to popular formation, and edema [9].

Dimethylhydrazines (DMH) is one of the most important hydrazine derivatives that exist in the environment due to its application in various human activities such as agriculture, industry, and medical activity. Moreover, dimethylhydrazine is utilized in the fuel manufacturing for jet-plane and rocket, in addition it considered as a plant growth enhancer, share in the chemical syntheses of feedstock, as additive in lubricants, and manufacturing of rubber [10]. Experimentally; subcutaneous or intra peritoneal injection of dimethylhydrazine leading to colorectal tumors in rat and mice, while chronic poisoning lead to hepatic fatty changes and elevation of alanine transaminase enzyme [11].

Azoxymethane (AOM) is a metabolite of the dimethylhydrazine (DMH) with chemical formula $C_2H_6N_2O$ as shown in (Fig. 1), has been used by several researchers to induce colon tumors in experimental rat. AOM-induced carcinoma has a transplantable nature and so metastasizes to the regional lymph nodes and then extends into the neighboring peritoneal tissues [12]. AOM-mediated carcinogenesis process included mutagenesis by induction of chromosomal damage and micronuclei (MN) cell formations with DNA damage in proliferated cells [13].

Moreover, AOM was also reported to cause reproductive toxicity, Kurus et al. [14] noted that AOM generated oxidative stress and pathological degenerative changes in the seminiferous tubules, such as atrophy, loss in the number of germ cells, arrested spermatogenic cell, and an increase in the connective tissue of the tunica albuginea. Furthermore, AOM treatment caused significantly lower testosterone levels.

In animal studies, recurrent exposure to DMH and its metabolite AOM are able to induce the procarcinogenesis effect after metabolic activation by alkylating chemical process forming the DNA reactive product. The AOM and the alkylated-DMH starting their mutation activities via the guanine base methylation at the position of N-7 in the mutated DNA. Then the pairing between the alkylated guanine and thymidine instead of cytosine was occurred by contributing proton that lead to a bases modification. Furthermore the next replication, mispairing of cytosine to adenine and guanine to thymine occurs, that causes DNA mutations [10].

Malignancies are commonly originated from the simple lining epithelia of ovaries, endometrium, mammary gland, prostate, lung, and colon that are usually metastasized to their regional lymph nodes and other organs. Later on; the fundamental incidence of the ovarian neoplasms was not primarily ovarian, however really metastasized from the neoplasms elsewhere in affected body, particularly the GIT [15]. The primarily originated ovarian cancer it featured as, large sized unilaterally localized lesion. While the metastasized carcinoma to ovary found small sized bilaterally localized [16,17]. The size of the primary colorectal cancer is generally smaller than that metastasized to ovaries and exhibit invasion of the muscularis propria [18,19].

Ovarian cancer yet the deadliest gynaecological tumors in human [20]. Endometriosis is the benign diseased form accompanied with malignant conversion and is the likely precursor lesion of the endometriosis accompanied ovarian carcinoma (EAOC) [21,22]. The reproductive organs tumor was detected in ovaries, uterus, cervix, vagina, and vulva with different grades of malignancy. These tumors lead to a great economic losses via infertility, production losses, and in severe cases death of the diseased animals [23,24].

Cytokeratins (CKs) are a group of 20 structural cytoskeletal proteins existed in the lining epithelia and neoplasms originated from the lining epithelia [18]. Expression of the CKs is commonly preserved by the cancer cells and thus, the particular anti cytokeratin antibodies greatly applied in the immunohistochemical diagnostic tools to detect the origin of the neoplastic cases, especially in metastasis. Cytokeratin-7 (CK-7) expression was detected in ovary, endometrium, mammary glands, lung, pancreas, skin, salivary gland and also considered as an intracytoplasmic marker in most adenocarcinomas [25,26]. The metastatic carcinoma of unknown origin is difficult to be diagnosed but in the last two decades the immunohistochemical protocols development aids in diagnosis of carcinoma via detection of several tumor markers [27].

Croton tiglium Linn plant recorded in the classic ancient books where it is related to five subfamily Crotonoideae contain 1300 species that are publicized worldwide mainly in subtropical and tropical areas. *C. tiglium* is a substantial element in *Crotonoideae* and its seeds are called *Crotonis Fructus* [28]. It is widely utilized therapeutically for homoeopathy, labour induction, gastrointestinal diseases treatment, ringworm, peptic ulcer, headache, rheumatoid arthritis, pain relief, and cancer treatment (Lima et al., 2018). The *C. tiglium*

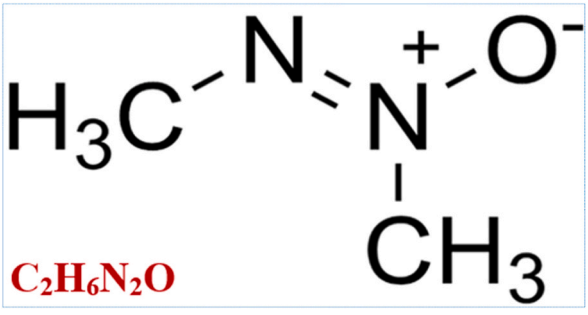

Fig. 1. The chemical formula of Azoxymethane.

extracts contains alkaloids as Magnolia; terpenoids as sesquiterpenoids and diterpenoids; fatty oils as oleic acid and palmitic acid; and also plants proteins. Pharmacologically; these metabolites has anti-inflammatory, antibacterial, analgesic, antifungal, and antitumor effects [28].

The metallic nanoparticles had been acquired a great interest due to their unique chemical and physical characters. That as a consequent to their huge surface/volume ratio depending on the nanoparticles shape and size. Silver nanoparticles (AgNPs) possess a unique characters as chemical stability and good conductivity and also its antiviral, antimicrobial, antioxidant, anti-inflammatory, and anticancer activity. All these characters has triggered the extensive use of the AgNPs [29,30].

The present study was aimed for studying of the toxic and carcinogenic effects of the AOM as metabolite of hydrazine derivative, which is existing as hazardous environment pollutant. Also determining the ameliorative effect of the *C. tiglium* L. seeds extract united

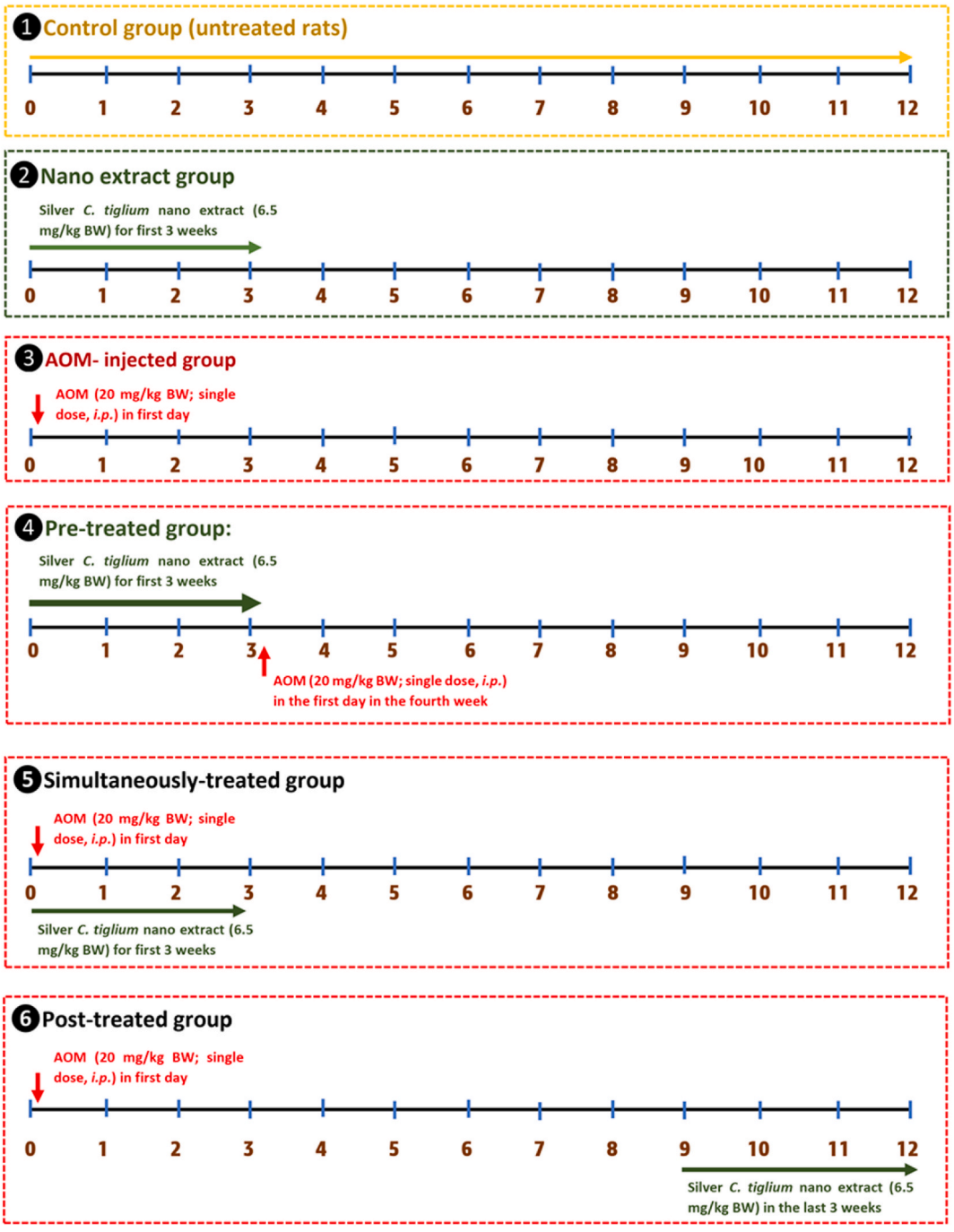

Fig. 2. Experimental scheme and treatments.

with the biosynthesized silver nanoparticles against the toxic and carcinogenic effects of the AOM as a metabolite from the dimethylhydrazine (DMH) derivatives. For achievement of this aim; histopathological examination, immunohistochemical detection for cytokeratin 7 (CK-7) as an ovarian and endometrial tumor marker, and hormonal studies were carried out.

2. Materials and methods

2.1. Extraction and phytochemical analysis of C. tiglium Linn seed

As published in our previous work Aboulthana et al. [31] Agricultural Research Centre, Giza, Egypt was the source for obtaining the *C. tiglium* seeds which were dried for 72 h in an incubator at 50 °C then grinded in electric mixer. The dried seeds powder had been subjected into the extraction using petroleum ether at 60–80 °C. Then filtered by Whatman filter paper and dried by a rotary evaporator at 45 °C under vacuum. This dried powder was reconstituted with distilled water.

The aqueous solution of the silver *C. tiglium* seeds nano-extract is fitted and standardized via the advanced and confirming tools which are applied orally through the usage of a gastric tube with a potion 6.5 mg/kg BW. This dose is 1/20 from the 50 % lethal dose (LD_{50}). the phytochemical analysis for the same samples of *C. tiglium* seeds extracts showed that this extract contains several phytochemical constituents like carbohydrates as glycosides, flavonoids, proteins, sterols as triterpenes, and finally alkaloids [31].

2.2. Preparation of silver C. tiglium seeds nano-extract

The nanoparticles of silver (Ag-NPs) were prepared according to Aboulthana et al. [31] via reduction of the silver nitrate ($AgNO_3$) by using ethylene glycol (EG) in polyol existence. By using the traditional mode, a 10 ml EG is reflux at 160 °C/25 min. 5 ml $AgNO_3$ solution was then added to a mixture from 0.15 M PVP in EG solution that included $MnCl_2$ as 0.03 mM that was poured into a flask for 10 min, then this mixture refluxed strongly and stirred at 160 °C/60 min. Thereafter cooling this mixture until reach to room temperature and then centrifuged at 5 min/3000 rpm and finally three time washing with acetone and ethanol was done. The AgNPs was gathered and then dehydrated in an oven at 70 °C. The gathered AgNPs was joined to the extract of *C. tiglium* seed with various concentrations to form the incorporated nano silver *C. tiglium* extracts.

2.3. Experimental scheme and treatments

An overall number of thirty-six female adult Wistar rats weighing between 120 and 150 g were used. The rats were provided with food and water ad libitum and kept under normal environmental and nutritional conditions at 25 ± 2 °C. The experiment was conducted following guidelines and ethical approvals from the animal welfare authorities of the National Research Centre, Dokki, Giza, Egypt (16116). AOM was injected intraperitoneally (*i.p.*) at a dose of 20 mg/kg body weight as a single dose in different experimental groups [32]. The experimental rats were randomly divided into six groups ($n = 6$) and fed a naturalistic diet with free access to clean water for 12 weeks as shown in Fig. 2.

- 1st group: untreated rats fed a normal diet for 12 weeks.
- 2nd group (Nano extract-group): These rats were fed a naturalistic diet and received daily oral administration of silver *C. tiglium* nano-extract at a dose of 6.5 ml/kg BW for the first 3 weeks, followed by a normal diet for 12 weeks.
- 3rd group (AOM-injected rats): Rats were injected (*i.p.*) with AOM at a dose of 20 mg/kg BW as a single dose and continued to be fed a normal diet for 12 weeks.
- 4th group (Pre-treated rats): Rats were orally administered silver *C. tiglium* nano-extract (6.5 ml/kg BW) daily for the first 3 weeks, then injected (i.p.) with AOM at a dose of 20 mg/kg BW as a single dose on the first day of the fourth week, and continued to be fed a normal diet for 12 weeks.
- 5th group (Simultaneously-treated group): These rats were injected (i.p.) with a single dose of AOM (20 mg/kg BW) on the first day of the experiment and treated with silver *C. tiglium* nano-extract daily during the first 3 weeks, followed by a normal diet for 12 weeks.
- 6th group (Post-treated rats): These rats were first treated with a single dose of AOM (20 mg/kg BW i.p.) on the first day of the experiment and then treated with silver *C. tiglium* nano-extract during the last 3 weeks of the experiment.

At the end of the experiment, the rats were anesthetized, and blood specimens were collected from the retro-orbital plexus in all groups. The blood samples were then centrifuged at 4000 rpm for 15 min to separate serum for hormonal analysis and protein measurement. Subsequently, all animals were sacrificed, and ovaries and uterus were collected for further investigations.

2.4. Histopathology examination

After sacrificing all experimental rats at the end of the 12-week experiment, post-mortem examinations were carried out. Tissue specimens from the ovaries and uteri of all rat groups were immediately collected. The collected tissue specimens were divided into two parts: one part was frozen (0.1-g tissue weight) for tissue homogenization for protein electrophoresis, and the other part was fixed in neutral buffered formalin (NBF) 10 % overnight. The tissue specimens were then transferred to 70 % ethanol to preserve the antigenic structure of the ovarian and uterine tumor marker antigen CK-7 from the effects of the formalin fixative. Routine tissue

processing, including dehydration, embedding in paraffin wax, and sectioning to a thickness of 4–5 μm, was performed to facilitate histopathology and immunohistochemistry protocols. Finally, the tissue slides were stained with a background stain of hematoxylin and eosin (H&E) for examination of cellular details [33].

2.5. Detection the tumor via immunohistochemical evaluation of (CK-7)

The prepared paraffin-embedded tissue blocks from ovarian and uterine tissue specimens are also suitable for the IHC protocol. Tissue blocks were sectioned at 4–5 μm and mounted on tissue slides coated with positive charges. The retrieval process for the CK-7 tumor marker antigen was performed using a heat-mediated antigen retrieval method. The slides were immersed in a retrieval solution consisting of a Tris/EDTA buffer at pH 9.0 before starting the IHC procedure, then autoclaved at 20–25 PSI pressure for 5 min. The tissue slides were incubated with a rabbit anti-CK-7 IgG monoclonal antibody preserved in a solution containing 0.01 % sodium azide, 59 % PBS, 40 % glycerol, and 0.05 % BSA (Bovine Serum Albumin) at a dilution rate of 1:8000 as recommended by the manufacturer. The antibody used was sourced from ABCAM Co, UK, with the clone number EPR17078.

The IHC kit used in the experiment is an HRP Polymer anti-polyvalent CRFTM (Di Amino Benzidine (DAB) stain peroxidase disclosure kit from Scy Tek Laboratories, USA. The specificity of the species in this kit is anti-mice, anti-rat, and anti-rabbit. The negative and positive control groups were included in the experimental design. The tissue slides under examination were stained with a counterstain as background using hematoxylin stain and then examined microscopically. The positive immunoreaction varied according to the intensity of antigen presence, resulting in a range of coloration degrees such as light brown, golden brown, and deep brown in the tested tissue specimens compared to the control negative and positive tissue slides [34].

2.6. Electrophoretic assays

2.6.1. Preparation of the tissue homogenates

Known weights (0.1g) of the ovarian and uterine tissue samples were taken from each rat and homogenized in 1 ml extraction buffer and then exposed to centrifugation at 10,000 rpm for 5 min. From each group, pooled samples were prepared by collecting equal volumes from the individual supernatants, which were then combined in one tube and used as one sample. The total protein concentration of all pooled specimens was quantified using the Bradford method [35]. All specimens were diluted with loading dye to ensure equal protein concentrations for electrophoretic assays in all wells.

2.6.2. Native electrophoretic protein patterns

Polyacrylamide Gel Electrophoresis (PAGE) was used to separate the local proteins, which were stained with Coomassie Brilliant Blue (CBB) [36] to assay the bands of protein that appeared as bluish bands. Additionally, Sudan Black B stain (SBB) was used to stain proteins [37] f for assaying lipid moiety, which appeared as black bands. Alizarin red stain was applied to assay calcium moiety, displaying as yellow bands [38].

2.6.3. Native electrophoretic isoenzyme patterns

The electrophoretic patterns for peroxidase enzyme (POX) and catalase enzyme (CAT) were analyzed through native gel incubation with a substrate of H_2O_2. The catalase enzyme types were illustrated as yellow bands when accepting the potassium iodide stain [39], while the peroxidase enzyme types were found as brown bands when accepting the benzidine stain [40]. The electrophoretic esterase (EST) enzyme patterns were analyzed through a native gel incubation with a conditioning buffer for enhancement of the activity of enzyme. A reaction mixture containing Fast Blue RR stain was used in gel (as a dye coupler) for staining the α- and β-naphthyl acetate as substrates to detect α and β-EST enzyme types, respectively [41]. The α-EST enzyme types were found as brown bands and the β-EST enzyme types were displayed as pink bands.

2.7. Reproductive hormones analysis

The levels of Follicle-Stimulating Hormone (FSH) and Luteinizing Hormone (LH) were assessed in rat sera using a quantitative Enzyme-Linked Immunosorbent Assay (qELISA) (Diagnostics Biochem., Canada Inc.) with a 14 pg/mL sensitivity, following the procedures described by Marshall (1975) and Uotila et al. (1981) respectively. The minimum measurable levels are $<$0.35 and 0.5 ng/mL, respectively. The level of 17β-estradiol (E2) was quantified using the qELISA assay kit (Diagnostics Biochem., Canada Inc.) with a 14 pg/mL sensitivity, following the method described by Ratcliffe et al. [42].

2.7.1. Data analysis

The hormonal analysis results were displayed as mean ± standard error (SE) and were statistically analyzed using a one-way analysis of variance (ANOVA) with the Statistical Package for Social Sciences (SPSS for Windows, version 11.0). This was followed by the Bonferroni test as a post-hoc analysis. Statistically significant differences among groups were considered when the "P" value was less than 0.05. For the electrophoresis images, the Quantity One software (Version 4.6.2) was used to analyze the relative mobility, band quantity, and the percentage of bands (B %) of the separated electrophoretic bands. The equation according to Nei and Li [43] was used to calculate the similarity index percentages (SI %) and percentage of genetic distance (GD %).

3. Results

3.1. Histopathological findings

Figs. 3 and 4 illustrated the histopathological changes in ovaries and uterus of control and treated rats, the ovary of the examined control rats appeared histologically normal where several stages of the growing follicles as multiple normal primordial and antral follicles were observed (Fig. (1A)). Uterus exhibited normal endometrial mucosa lined with intact simple columnar epithelium associated with normal intact uterine glands (1B). Furthermore, the ovary of the silver *C. tiglium* nano extract displayed normal histological tissue architecture with several follicular stages (1C). Also, uterus illustrated normal active and coiled uterine glands (1D). Otherwise, the ovarian corpora lutea of AOM-treated rats illustrated some areas of focal coagulative necrosis in their lutein cells which also surrounded with other severely degenerated lutein cells (1E). Uterus showed existence of large endometriotic cyst of a dysplastic mass of abnormal cell aggregations and uterine glands detected in the myometrial layer (1F).

While, the ovarian tissue of silver *C. tiglium* nano extract-pre-treated exhibited normal active corpora lutea and normal antral follicles were found (2G), in addition; intact endometrial lining epithelium and normal intact uterine glands were observed which also associated with mild spaces of degeneration (2H). In addition, severe degenerative changes and necrosis in some of the ovarian follicles granulosa cell layer were found in the ovarian tissue of the silver nano-extract simultaneous-treated rats (2I). In addition, the uterine tissue showed multifocal metaplasia in endometrial epithelium where their nature transformed from simple columnar into stratified columnar epithelium in comparison with the adjacent normal simple columnar endometrial epithelium (2J). The ovary of this silver *C. tiglium* nano-extract t-post-treated rats illustrated normal antral follicles and otherwise, corpora lutea displayed mild vacuolar degeneration in their lutein cells (2K). The uterine tissue showed a stage of active progestational proliferation in endometrium accompanied with mild focal desquamation in endometrial lining epithelium (2L).

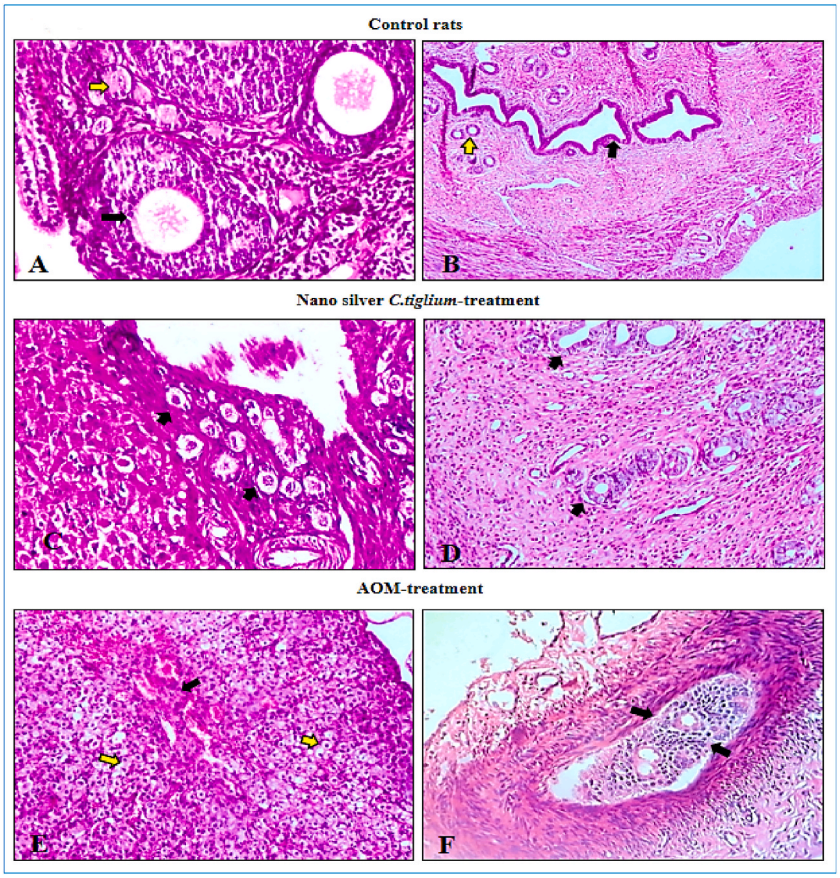

Fig. 3. Illustrated the histological finding in ovary of rats treated by Azoxymethane with and without Silver *C. tiglium* nano-extract. Control group: A: ovary of rat showed completely normal antral follicles (black arrow) and normal primordial follicles (yellow arrow) H&E X 200. B: uterus showed normal endometrial lining epithelium (black arrow) and normal intact uterine glands (yellow arrow) H&E X 40. Silver *C. tiglium* nano-extract -treated rats: C: normal primordial follicles was exhibited H&E X 200. D: Uterus exhibited normal active coiled uterine glands H&E X 100. AOM-treated rats: E: Ovary displayed focal coagulative necrosis in in the lutein cells of corpus luteum (black arrow) surrounded with other severely degenerated lutein cells (yellow arrows) H&E X 100. F: large endometriotic cyst of a dysplastic mass of abnormal cell aggregations and uterine glands appeared in the myometrial uterine layer was observed (black arrows) H&E X 100.

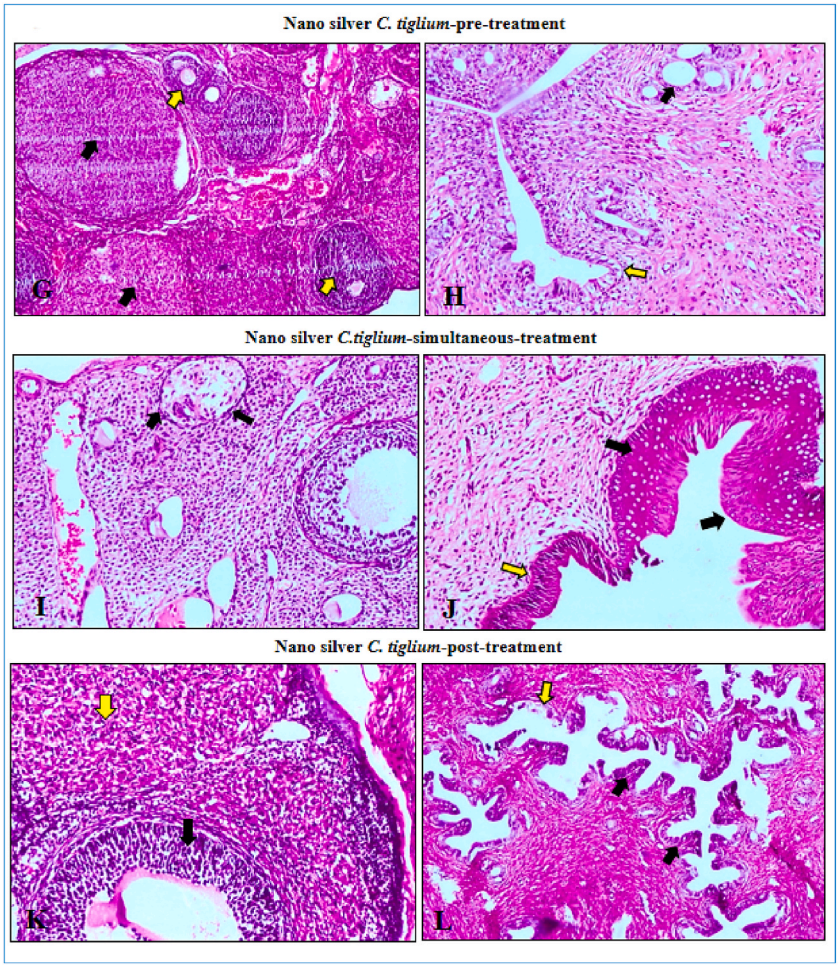

Fig. 4. Exemplified the histological finding in ovary of rats treated by Azoxymethane with and without Silver *C. tiglium* nano-extract. Silver *C. tiglium* nano-extract -pre-treated rats: Silver *C. tiglium* nano-extract -pre-treated rats (G): ovary displayed completely normal corpora lutea (black arrows) and normal antral follicles (yellow arrows) H&E X 40. (H): Intact healthy endometrial epithelium was displayed with mild spaces of degeneration (yellow arrow) associated with normal intact uterine glands (black arrow) H&E X 100. Silver *C. tiglium* nano-extract -simultaneous-treated rats (I): Ovary illustrated severe degeneration and necrosis in the granulosa cells of some of antral follicle (black arrows). (J): Multifocal metaplastic changes in endometrial epithelium, which changed to stratified squamous columnar (black arrows) as compared with simple columnar endometrial epithelium (yellow arrow) H&E X 100. Silver *C. tiglium* nano-extract -post-treated rats (K): Ovary of rat showed completely normal antral follicles (black arrow) and corpora lutea showed mild vacuolar degeneration (yellow arrow) H&E X 100. (L): Normal uterus in the active progestational proliferation stage of endometrium (black arrows) associated with mild exfoliation in some areas of endometrial lining epithelium (yellow arrow) H&E X 40.

3.2. IHC findings

The IHC protocol was used in our experiment to determine the presence of the CK-7 marker in the ovaries and uterus of the control and treated rats, as shown in Figs. 5 and 6. The IHC findings revealed that both control rats and rats treated with nano silver *C. tiglium* extract showed negative immunoreactivity in the ovarian and uterine tissues due to the absence of the CK-7 marker in the cells of these tissues (3M, 3N, 3O, and 3P). In contrast, samples from AOM-treated rats exhibited moderate positive immunoreactivity for the intracytoplasmic localization of the CK-7 marker antigen. This was observed in the interstitial hilus cells of the ovarian stroma that were adjacent to the blood capillaries near the ovarian corpus luteum (3Q). Additionally, moderate positive immunoreactivity was observed intracytoplasmically in the detached endometrial cells that were aggregated in the uterine lumen (3R).

Furthermore, in the fourth group, samples illustrated a mild positive immunoreaction for the presence of the CK-7 marker, which was detected perivascularly in the cytoplasm of a few of the interstitial hilus cells of the ovarian stroma (4S) and also detected per-iglandularly in the cytoplasm of the interstitial stromal cells in the uterine lamina propria submucosa (4T). In addition, the samples of silver nano-extract simultaneous-treated rats displayed a moderately positive immunoreaction as a result of the intracytoplasmic detection of the CK-7 antigen in the interstitial hilus cells in the ovarian stroma, which adhered to the well-developed corpus luteum (4U). Correspondingly, mild localization for the CK-7 antigen intracytoplasmically in a few of the perivascular endometrial interstitial

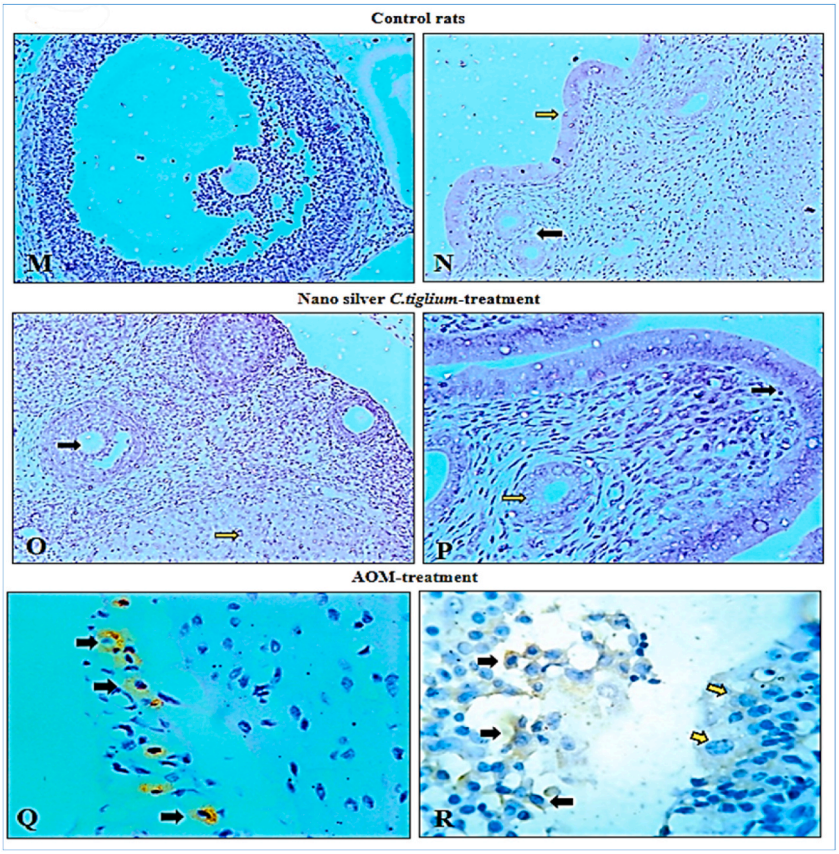

Fig. 5. Detection of the ovarian and uterine tumor marker CK-7 by IHC technique in rats treated Azoxymethane with and without Silver *C. tiglium* nano-extract. Control rats (M & N): Negative immunoreaction against the CK-7 marker antigen was observed in normal mature ovarian follicle and in normal intact endometrial epithelium (yellow arrow-DAB X 100). Silver *C. tiglium* nano-extract -treated rats (O & P): Also negative immunoreaction against CK-7 marker antigen was observed in normal antral ovarian follicle (black arrow) and normal corpus lutium (O; yellow arrow). DAB X 100. In addition, normal intact endometrial epithelium (black arrow) associated with normal uterine glands (P; yellow arrow). DAB X 200. AOM-treated rats (Q & R): Moderately positive immunoreaction against CK-7 marker antigen was observed in the interstitial hilus cells of the ovarian stroma adjacent to the corpus lutium (Q; black arrow) and also detected in the detached endometrial cells which found aggregated in the uterine lumen (R; black arrows). DAB X 400.

cells in the stroma of the submucosal layer (4V). Besides, the negative immunoreaction due to the absence of the CK-7 marker in the mature ovarian follicle granulosa cells was found in nano silver *C. tiglium* extract-post-treated rats and observed in the luteal cells of the adjacent corpus luteum (4W). On the other hand, a moderately positive immunoreaction was detected intracytoplasmically in the detached endometrial cells that aggregated in the narrow uterine lumen (4X).

3.3. Detection of the protein, lipids, calcium, and isoenzymes patters via electrophoretic assays

3.3.1. Electrophoretic protein pattern

Figure (7A) ovaries of control rats illustrates the electrophoretic representation of the native protein pattern showing 6 bands (Rfs 0.20, 0.40, 0.60, 0.72, 0.77, and 0.96; Qty 51.65, 48.61, 48.27, 100.00, 62.91, and 65.10; B% 13.72, 12.91, 12.82, 26.56, 16.71, and 17.29, respectively). The common three bands were identified at Rfs 0.20, 0.77, and 0.96. Physiological alterations were observed in AOM-treated group. 3 normal protein bands were hidden and one characteristically abnormal band appeared at Rfs 0.53 (Qty 64.24; B % 20.33). As a result, the SI values (SI = 60.00 %) in ovaries of the AOM-treated group decreased as compared with the control rat group. Administration of the silver *C. tiglium* nano-extract in all therapeutic modes (pre-, simultaneous-, and post-treated groups) enhanced the protein pattern through hiding a characteristic band and retrieve two normal bands detected at Rfs 0.41 and 0.74 in the pre-treated group with Qty 37.76 and 100.00 (B% 11.87 and 31.44), in the simultaneous-treated group with Qty 41.24 and 100.00 (B% 11.90 and 28.86), and in the post-treated group with Qty 42.11 and 100.00 (B% 13.43 and 31.88, respectively). Therefore, these groups were physiologically similar to the control rats by 90.91 %.

Fig. (7B) shows that the uterus of the control rat group displayed a native protein pattern consisting of 5 bands (Rfs 0.13, 0.32, 0.54, 0.79, and 0.92; Qty 49.36, 100.00, 89.26, 24.91, and 83.47; B% 14.23, 28.82, 25.72, 7.18, and 24.05, respectively). Three prominent bands were identified (Rfs 0.32, 0.79, and 0.92), with no characteristic bands detected. Injection of AOM led to several physiological

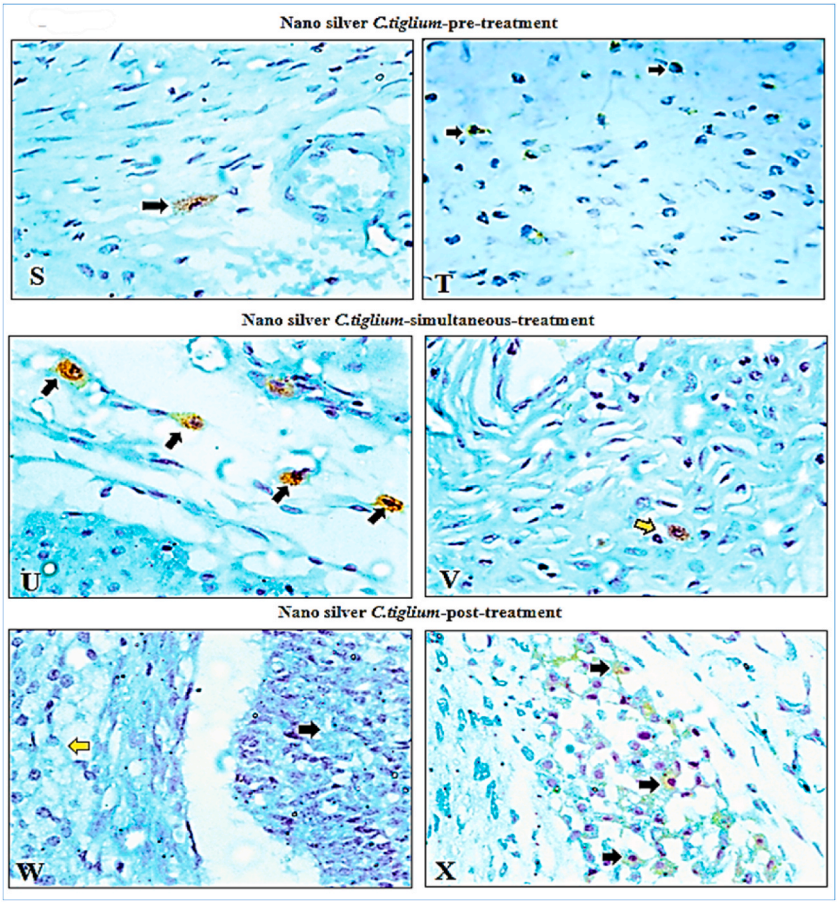

Fig. 6. Detection of the ovarian and uterine tumor marker CK-7 by IHC technique in rats treated Azoxymethane with and without Silver *C. tiglium* nano-extract. Silver *C. tiglium* nano-extract -pre-treated rats (S & T): Mild positive immunoreaction toward the CK-7 marker antigen was detected in few of the interstitial hilus cells of the ovarian stroma (S; arrow) and also detected periglandular in the uterine stroma interstitial cells in lamina propria submucosa (T; arrows). DAB X 400. Silver *C. tiglium* nano-extract -simultaneous-treated rats (U & V): Moderately positive immunoreaction was detected in the interstitial hilus cells of the ovarian stroma adjacent to the well-developed corpus lutium (U; black arrows) and also mild detected in few of the perivascular interstitial hilus cells in the submucosal layer (V; yellow arrow). DAB X 400. Silver *C. tiglium* nano-extract -post-treated rats (W): Normal granulosa cells in mature ovarian follicle (black arrow) adjacent to normal lutein cells of corpus lutium (yellow arrow) showed negative immunoreaction against CK-7 marker antigen. DAB X 400. (X): Moderately positive immunoreaction was detected in the detached endometrial cells that aggregated in the narrow lumen of uterus. DAB X 400.

changes resulting in the masking of two normal protein bands and the appearance of two abnormal ones at Rf 0.46 and 0.68 (Qty 61.73 and 45.81; B% 15.54 and 11.53, respectively). As a result, the SI values (SI = 60.00 %) decreased in the brain of the AOM-treated group compared to the control group. Pre-treatment with silver *C. tiglium* nano-extract improved the protein pattern by restoring two normal bands (Rfs 0.14 and 0.54; Qty 47.12 and 55.41; B% 15.27 and 17.96, respectively) while masking the abnormal ones. Application of the nano silver *C. tiglium* extract in the simultaneous-treated group minimized the electrophoretic disturbances by restoring just a single normal band (Rf 0.13; Qty 71.48 and B% 23.22) while masking the other abnormal ones. Post-treatment with nano silver *C. tiglium* extract showed a lower ameliorative effect compared to the other silver *C. tiglium* nano-extract treated groups by restoring just one naturalistic band (Rf 0.14; Qty 72.64 and B% 19.47) without masking the abnormal ones that exist at Rfs 0.47 and 0.64 (Qty 76.09 and 53.73; B% 20.39 and 14.40, respectively). Therefore, SI values increased in the nano silver *C. tiglium* extract simultaneous-treated and post-treated groups (SI = 80.00 and 72.73 %), respectively.

3.4. Electrophoretic lipid moiety of the native protein pattern

Figure (7C) shows that the lipid moiety of the native protein pattern in the ovaries of the control rats was represented by three bands (Rfs 0.20, 0.77, and 0.97; Qty 8.93, 9.86, and 11.91; B% 29.10, 32.13, and 38.77, respectively). Only one prominent band was detected at Rf 0.97. In the AOM-treated group, the physiological changes in the lipid moiety of the native protein pattern were demonstrated by the absence of two normal protein bands. No characteristic bands were identified. Therefore, the similarity of this electrophoretic pattern in the ovaries of the AOM-treated rats decreased compared to the control rats (SI = 50.00 %). Administration of

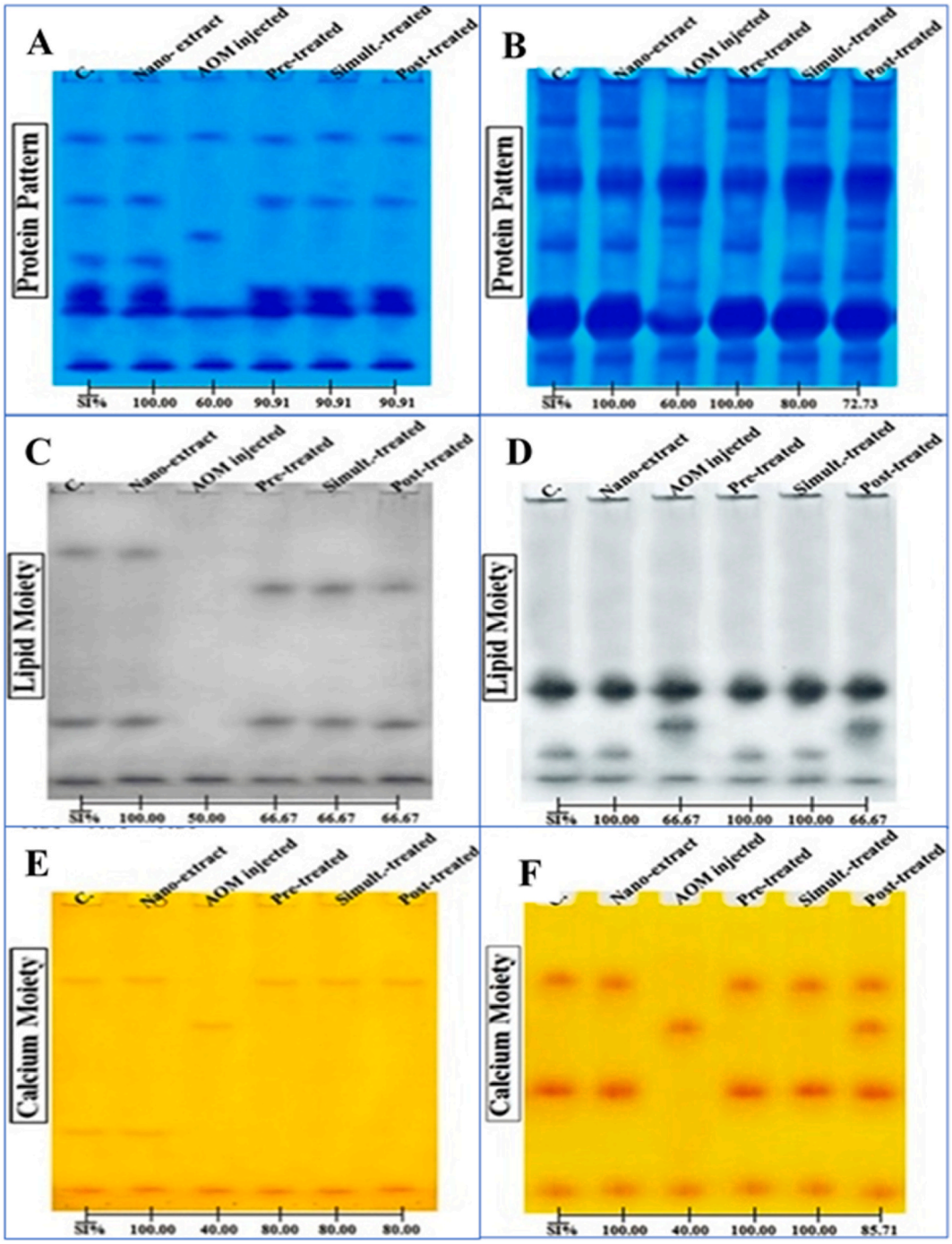

Fig. 7. Native electrophoretic protein, lipid, and calcium patterns showing efficiency of Silver *C. tiglium* nano-extract against the physiological alterations induced by Azoxymethane (AOM) in ovary and uterine tissue of rats. The original image of electrophoresis bands is represented in the supplementary materials.

nano silver *C. tiglium* extract in all therapeutic modes (pre-treated, simultaneous-treated, and post-treated groups) ameliorated the protein pattern by restoring just one normal band recognized at Rf 0.77 in the pre-treated group with Qty 11.27 (B% 35.77), in the simultaneous-treated group with Qty 10.01 (B% 31.02), and in the post-treated group with Qty 10.03 (B% 33.34) with the presence of one abnormal band recognized at Rf 0.32 in the pre-treated group with Qty 9.65 (B% 30.63), in the simultaneous-treated group with Qty 11.22 (B% 34.77), and in the post-treated group with Qty 8.04 (B% 26.72). Therefore, these groups were physiologically analogous to the control by 66.67 %.

Figure (7D) in the uterus of the control rats showed that the lipid moiety of the native protein pattern was illustrated by three bands (Rfs 0.64, 0.85, and 0.94; Qty 34.26, 11.65, and 12.42; B% 58.74, 19.97, and 21.29, respectively). Two prominent bands were detected (Rfs 0.64 and 0.94), and no characteristic bands were observed. AOM caused abnormal physiological modifications in this native pattern, manifested by the disappearance of one normal band and the presence of an abnormal band (Rf 0.76; Qty 20.74 and B% 33.76). The SI value (SI = 66.67 %) decreased in the uterus of the AOM-treated group compared to the control rats. Administration of nano silver *C. tiglium* extract in the pre-treated and simultaneous-treated groups improved this pattern by masking the abnormal band and restoring the normal one at Rf 0.85 with Qty 10.74 (B% 19.28) in the pre-treated group and Qty 8.77 (B% 15.13) in the simultaneous-treated group. These groups were completely similar to the control (SI = 100.00 %). In the post-treated rats, the nano silver *C. tiglium* extract did not improve this native pattern. Therefore, the electrophoretic pattern in this rat group was physiologically similar to the control by 85.71 %.

3.5. Electrophoretic calcium moiety of the native protein pattern

Figure (7E) displays the representation of the calcium moiety of the native protein pattern in the ovaries of the control rats. In the control rat group, three bands were specified at Rfs 0.26, 0.75, and 0.94, with quantities of 1.56, 1.75, and 6.15, and percentages of 16.52, 18.51, and 64.97, respectively. Only one popular band was recognized at Rf 0.94. In the AOM-treated group, two normal bands were hidden, and one abnormal band was distinguished at Rf 0.40, with a quantity of 4.21 and a percentage of 41.74. This resulted in the lowest SI value (SI = 40.00 %) in the ovaries of the AOM-treated rat group compared to the control rat group. The treatment with silver *C. tiglium* nano extract in all therapeutic modes (pre-treated, simultaneous-treated, and post-treated groups) improved the protein pattern by concealing the characteristic band and retrieving only one normal band specified at Rf 0.26 in the pre-treated rat group with a quantity of 1.77 and a percentage of 20.45, in the simultaneous-treated group with a quantity of 1.76 and a percentage of 19.72, and in the post-treated group with a quantity of 3.04 and a percentage of 28.02. Therefore, these groups were identical to the control rat group by 80.00 %.

Figure (7F) in the uterus of control rat group, it was detected that the calcium moiety of native protein pattern was existed as 3 bands (Rfs 0.24, 0.60, and 0.93; Qty 11.73, 15.10, and 11.50; B% 30.59, 39.41, and 30.01 respectively). One common band was distinguished at Rf 0.93. No specific bands were observed. The AOM injection caused physiological abnormalities in this native pattern, with two naturalistic bands being hidden and the existence of one extraordinary band detected at Rf 0.39 (Qty 12.11 and B% 46.31). Therefore, the minimal SI value (SI = 40.00 %) was observed in uterus of AOM-treated group in comparison with the control rat group. Application of the nano silver *C. tiglium* extract in both of pre-treated and simultaneous-treated groups ameliorated this pattern by concealing the abnormal band and retrieving the other two normal bands that specified at Rfs 0.26 and 0.60 with Qty 12.21 and 14.70 (B% 31.55 and 37.98) in the pre-treated group and Qty 12.58 and 15.38 (B% 31.81 and 38.89), respectively in the simultaneous-treated group. Therefore, these groups were completely similar as compared the control rats (SI = 100.00 %). In the post-treated group, the nano silver *C. tiglium* extract exhibited a lower amelioration on this native pattern by restoring the two normal ones

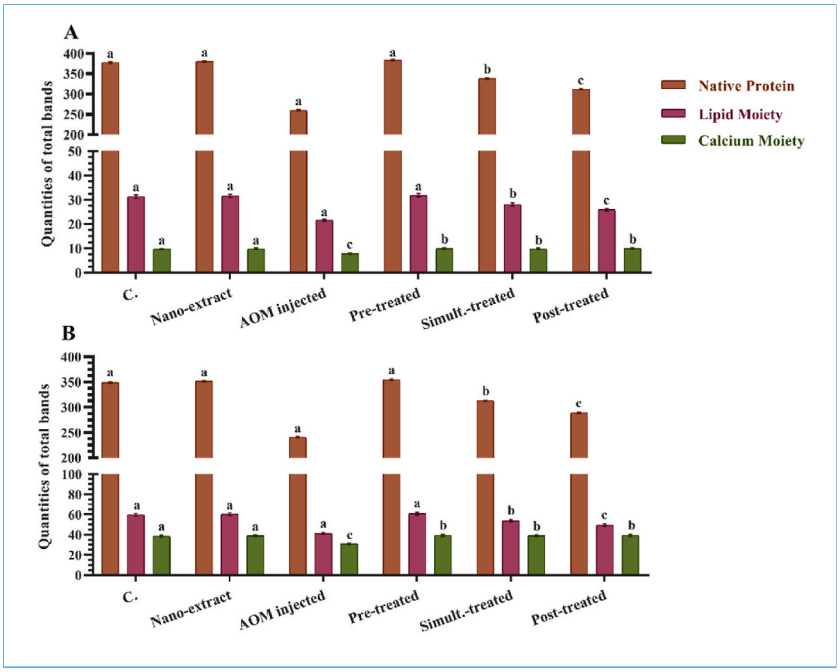

Fig. 8. Quantitation of the overall bands of native electrophoretic protein, lipid, and calcium patterns showing efficiency of Silver *C. tiglium* nano-extract to ameliorates the azoxymethane (AOM) physiological alteration effects in A) ovary and B) uterus.

that specified at Rfs 0.26 and 0.61 (Qty 11.56 and 14.19; B% 23.18 and 28.45, respectively) with no hiding the abnormal one that present at Rf 0.40 (Qty 11.12 and B% 22.29). Thus, the SI value in this rat group is equal to that in the AOM-treated group as compared to the control rats. The overall band quantities of the native electrophoretic lipid, protein, and calcium patterns illustrated in Fig. 8.

3.5.1. Electrophoretic isoenzyme patterns

3.5.1.1. Electrophoretic catalase (CAT) pattern. The CAT isoenzyme pattern in ovaries of the control rat group as shown in Figure (9A) consisted of 3 types (Rfs 0.26, 0.61, and 0.93; Qty 15.43, 22.71, and 19.48; B% 26.78, 39.42, and 33.80, respectively). The specification of the two CAT types (CAT1 and CAT3) was done at Rfs 0.26 and 0.93 are deemed as popular bands, with no characteristically bands detected. In AOM-treated group, the observation of qualitative abnormalities was pronounced including the absence of one CAT type (CAT2) and in addition, the appearance of one abnormal band was detected (Rf 0.44; Qty 21.37; B% 40.50). Consequently, the AOM-treated group recorded the lowest SI value (SI = 66.67 %) as matched with the control group. However, pre-treatment with nano silver *C. tiglium* extract enhances this isoenzyme pattern by returning the CAT type into normal (CAT2) at Rf 0.61 (Qty 22.91; B% 39.96) and hiding the abnormal one, resulting in a CAT isoenzyme pattern in the nano-extract pre-treated group that was analogous completely as matched with the control rats (SI = 100.00 %). Administration of silver nano-extract in simultaneous- and post-treated groups minimized the deleterious effects induced by AOM by concealing the abnormal band and retrieved the normal one that specified at Rf 0.61 with Qty 17.69 (B% 26.68) in the simultaneous-treated group and Qty 17.79 (B% 26.30) in the post-treated group. Therefore, these groups were physiologically identical to the control rats by 85.71 %.

In uteri of the control rat group in Figure (9C), it was found that the CAT isoenzyme pattern consisted of 3 types (Rfs 0.27, 0.56, and 0.88; Qty 8.60, 23.28, and 21.50; B% 16.11, 43.62, and 40.28, respectively). The two types of CAT enzyme (CAT2 and CAT3) were specified at Rfs 0.56 and 0.88 are deemed as popular bands. No characteristically, bands were detected. The injection of AOM leads to physiological abnormalities, leading to the disappearance of CAT1 without the presence of abnormal bands. As a result, the value of the SI% decreased to 80.00 % as compared with the control rat group. The application of silver nano-extract in the pre-treated and simultaneous-treated groups improved this pattern by returning the CAT1 into normal which detected at Rf 0.27 with Qty 8.50 (B% 16.57) in the pre-treated group and Qty 8.19 (B% 15.86) in the simultaneous-treated group. Therefore, these groups were qualitatively analog with the control rats by 100.00 %. However, in the post-treated group, the nano-extract was unable to improve this isoenzyme

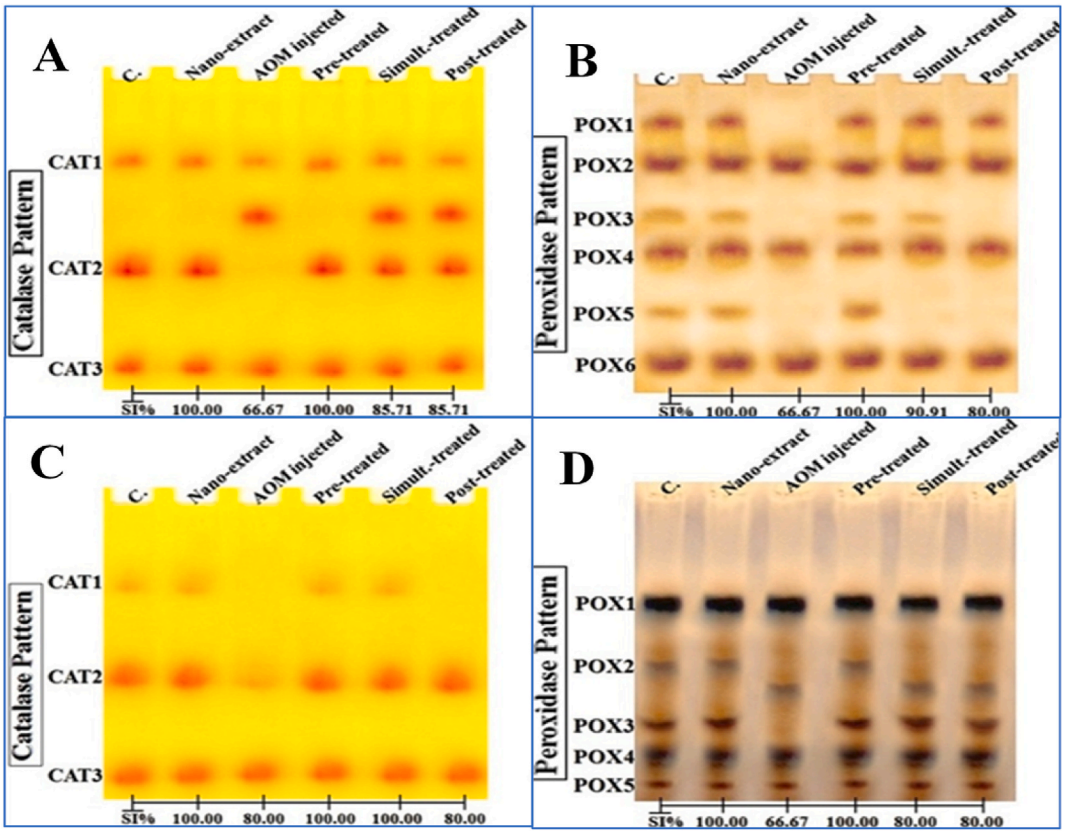

Fig. 9. Native electrophoretic isoenzymes patterns showing efficiency of Silver *C. tiglium* nano-extract against the physiological alterations induced in catalase (CAT) and peroxidase (POX) enzymes by Azoxymethane (AOM) in ovary, and uterine tissues of rats. The original image of electrophoresis bands is represented in the supplementary materials.

pattern. As a result, this group showed an electrophoretic pattern that was physiologically identical to the control rats by 80.00 % as in the AOM-treated rats.

3.5.1.2. Electrophoretic peroxidase (POX) pattern. The POX isoenzyme pattern in the ovary of control rats was illustrated in Figure (9B) which displayed by 6 types (Rfs 0.12, 0.25, 0.41, 0.52, 0.70, and 0.87; Qty 12.35, 14.81, 4.34, 14.27, 6.59, and 6.18; B% 21.10, 25.30, 7.41, 24.38, 11.26, and 10.55, respectively). The common bands POX2, POX4, and POX6 were specified at Rfs 0.25, 0.51, and 0.87. No characteristical bands were detected. In the AOM-treated group, the POX isoenzyme pattern showed qualitative abnormalities, with the POX1, POX3, and POX5 types hidden and no abnormal bands present. The obtaining of the lowest SI value (SI = 66.67 %) has occurred in this group as matched with the control rats. The nano silver *C. tiglium* extract improved the isoenzyme pattern in the pre-treated rats by restoring the absence of POX1, POX3, and POX5 which were specified at Rfs 0.12, 0.41, and 0.70 (Qty 13.31, 6.72, and 10.22; B% 21.07, 10.64, and 16.19, respectively). The POX isoenzyme pattern in the nano-extract pre-treated group was similar to that in the control rats by 100.00 %. In the simultaneous-treated group, only the two types POX1 and POX3 were restored and detected at Rfs 0.11 and 0.41 (Qty 13.43 and 5.76; B% 24.13 and 10.35, respectively). Therefore, this isoenzyme pattern was physiologically similar to the control by 90.91 %. In the post-treated group, only one POX type (POX1) was restored and identified at Rfs 0.11 (Qty 12.36; B% 24.14). Thus, this isoenzyme pattern was analogous physiologically by 80.00 % when compared with the control rats.

The uteri of the control rats were displayed in Figure (9D), it was pronounced that; the POX isoenzyme pattern was exhibited by 5 types (Rfs 0.36, 0.55, 0.74, 0.84, and 0.93; Qty 10.46, 8.36, 8.41, 11.05, and 6.62; B% 23.29, 18.62, 18.74, 24.62, and 14.73, respectively). POX1, POX4, and POX5 were specified at Rfs 0.36, 0.84, and 0.93 are deemed as popular bands. No characteristic bands were detected. In AOM-treated group, the POX isoenzyme pattern revealed physiological changes which were represented by hiding both POX2 and POX3 with the existence of a single abnormal band at Rf 0.62 (Qty 8.66 and B% 28.58). As matched with the control rats, the AOM-treated group had the lowest SI value (SI = 66.67 %). The nano silver *C. tiglium* extract improved this isoenzyme pattern in the pre-treated group by restoring the absence of both POX2 and POX3 that specified at Rfs 0.55 and 0.74 (Qty 5.70 and 10.06; B% 12.58 and 22.19, respectively). Therefore, the POX isoenzyme pattern in the nano silver *C. tiglium* extract pre-treated group was completely congruent with that in control rats (SI = 100.00 %). Treatment of silver *C. tiglium* nano-extract in the simultaneous- and post-treated groups showed the same (lower) ameliorative effect in this isoenzyme pattern by retrieving only POX3 to a normal level that detected at Rf 0.73 with Qty 13.06 (B% 25.26) in the simultaneous-treated group and Qty 11.24 (B% 24.88) in the post-treated rats without concealing the abnormal band. Therefore, these groups were identically (SI = 80.00 %) when compared to the control rat.

3.5.1.3. Electrophoretic esterase (EST) pattern. The electrophoretic pattern of the α-EST isoenzyme in ovaries of the control rats as in Figure (10A), illustrated 2 types (Rfs 0.17 and 0.81; Qty 33.26 and 27.14; B% 55.06 and 44.94, respectively). Both types of α-EST are

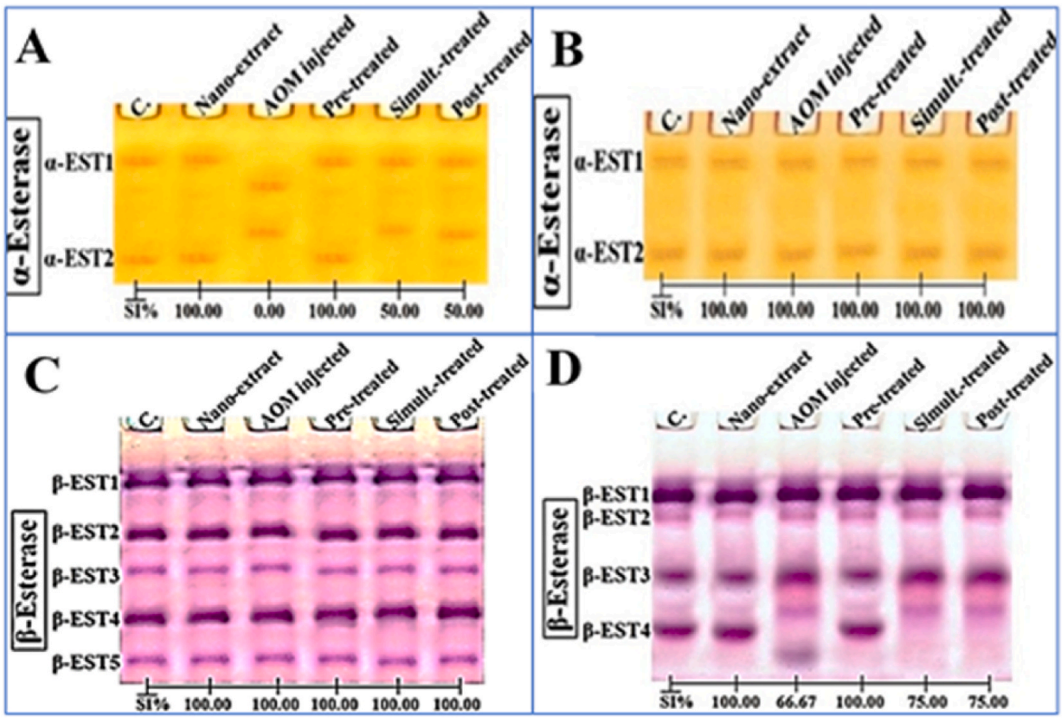

Fig. 10. Native electrophoretic isoenzymes patterns showing efficiency of Silver *C. tiglium* nano-extract against the physiological alterations induced in α-esterase (α-EST) and β-esterase (β-EST) by Azoxymethane (AOM) in ovary and uterine tissue of rats. The original image of electrophoresis bands is represented in the supplementary materials.

deemed common bands, with no characteristical bands detected. In AOM-treated group, neither qualitative nor quantitative abnormalities were found in α-EST isoenzyme pattern. Treatment of the silver nano-extract either single or combined with AOM in all silver *C. tiglium* nano-extract treated groups showed no variations from the control group in this isoenzyme pattern. Thus, the α-EST isoenzyme pattern in every treated rat group was physiologically analogous to the control rat group by 100.00 %.

The α-EST isoenzyme pattern in the uteri of the control rats as represented in Figure (10B), was illustrated by 2 types (Rfs 0.26 and 0.86; Qty 9.18 and 10.35; B% 46.98 and 53.02, respectively). No common bands were noticed, but there is one characteristic band specified in the AOM-treated group at Rf 0.40 (Qty 18.79 and B% 71.78). While, the AOM injection affected the α-EST isoenzyme pattern and led to qualitative abnormalities which were represented by the disappearance of both α-EST types and appearance of two abnormal bands at Rfs 0.40 and 0.66 (Qty 18.79 and 7.39; B% 71.78 and 28.22, respectively). Therefore, there is no resemblance between the AOM-treated rats and the control rats (SI = 0.00 %). The nano silver *C. tiglium* extract diminished the adverse effect induced in this isoenzyme pattern by AOM in the pre-treated rats by retrieving the absence of α-EST types that were detected at Rfs 0.24 and 0.85 (Qty 5.43 and 7.27; B% 42.74 and 57.26, respectively). Therefore, the α-EST isoenzyme pattern in the nano-extract pre-treated group was completely congruent to that in the control rats (SI = 100.00 %). Administration of silver nano-extract in simultaneous and post-treated groups showed the same (lower) ameliorative effect in this isoenzyme pattern by restoring only one normal (α-EST type (α-EST1) specified at Rf 0.26 with Qty 14.48 (B% 46.46) in the simultaneous-treated group and Qty 22.05 (B% 60.68) in a post-treated rat group without concealing of the abnormal band. Therefore, these rat groups were physiologically nearly to be similar to the control rat with the same percent (SI = 50.00 %).

The electrophoretic β-EST isoenzyme pattern in ovaries of the control rats was exhibited in Figure (10C) and consisted of 5 types (Rfs 0.20, 0.40, 0.54, 0.72, and 0.89; Qty 15.96, 14.55, 9.44, 17.18, and 10.02; B% 23.77, 21.66, 14.06, 25.59, and 14.92, respectively). All the β-EST types are deemed common bands, and no characteristical bands were noticed. In AOM injected group, neither qualitative nor quantitative abnormalities were detected in the β-EST isoenzyme pattern. Application of the silver nano-extract either alone or combined with the AOM in all nano-extract treated groups led to no variations from the control rats in this pattern. Therefore, the β-EST isoenzyme pattern in all treated rat groups was completely congruent to the control rat group (SI = 100.00 %).

The β-EST isoenzyme pattern in uteri of the control rats as shown in Figure (10D) consisted of 4 types (Rfs 0.26, 0.34, 0.58, and 0.81; Qty 28.51, 7.98, 21.06, and 22.25; B% 35.73, 10.00, 26.39, and 27.88, respectively). Both β-EST1, β-EST2, and β-EST3 were specified at Rfs 0.26, 0.34, and 0.58 are deemed popular bands. In the AOM-treated group, there was only one characteristical band detected at Rf 0.91 (Qty 15.99 and B% 18.28). The injection of AOM led to abnormal physiological changes in the β-EST isoenzyme pattern, resulting in the hiding of the only β-EST4 type and the semblance of another two abnormal bands at Rfs 0.73 and 0.91 (Qty 10.92 and 15.99; B% 12.49 and 18.28, respectively). Matching with the control rats, the AOM-treated rats had the lowest SI value (SI = 66.67 %). The silver *C. tiglium* seeds nano-extract diminished the adverse effect induced by AOM in the pre-treated group by concealing the abnormal bands and retrieving the absence of β-EST4 type identified at Rf 0.80 (Qty 23.52; B% 29.25). Therefore, the

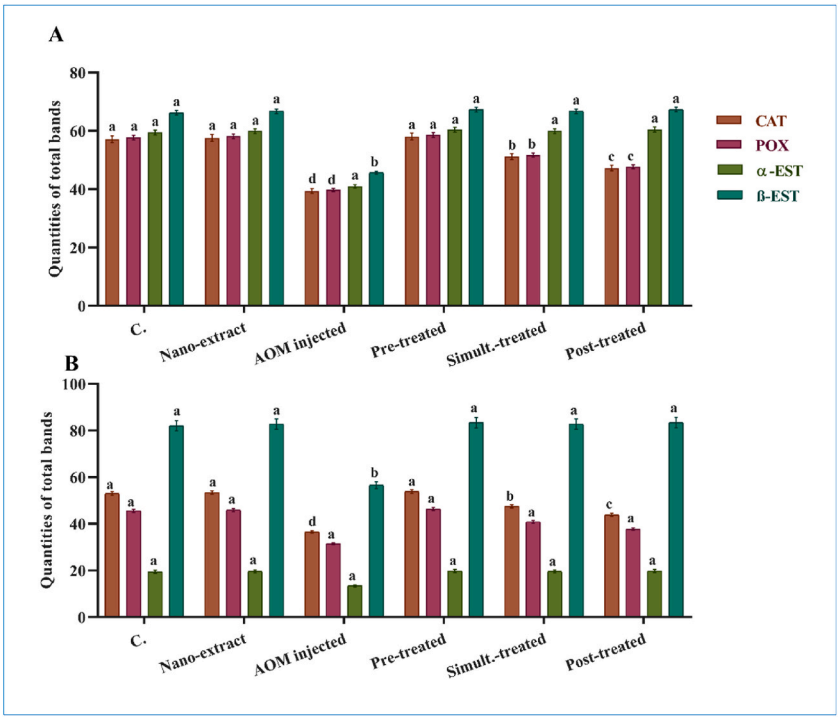

Fig. 11. Quantitative of total bands of isoenzyme (CAT, POX, α-EST, β-EST) patterns displayed the efficiency of Silver *C. tiglium* nano-extract against the physiological changes induced by the azoxymethane (AOM) in **A)** ovary and **B)** uterine tissue of rats.

β-EST isoenzyme pattern in the nano-extract pre-treated rats was completely congruent to the control rats (SI = 100.00 %). Administration of silver nano-extract in simultaneous- and post-treated groups showed a similar (lower) ameliorative effect in this isoenzyme pattern by concealing the characteristical band only with no retrieving of the absence of normal β-EST type. Therefore, these rat groups were physiologically congruent to the control with the same percent (SI = 75.00 %). The total band quantities of isoenzyme (CAT, POX, α-EST, β-EST) are illustrated in Fig. 11.

3.6. Impact of AOM and C. tiglium seed extract on reproductive related-hormones

The reproductive hormonal levels of FSH, LH, and E2, which are illustrated in Figure (12 A, B, and C), were significant at ($P \leq 0.05$) elevated in sera of AOM-injected rats as matched with the control rat group. The application of the silver *C. tiglium* seeds nano-extract is significant at ($P \leq 0.05$) and decreased these hormonal levels in all nano-extract-treated rat groups as matched with the AOM-injected rat group. However, it retrieves their levels to normal in the nano-extract pre-treated group.

4. Discussion

The idea of using the neoplastic preventive diet containing natural plant products is gaining increased attention. In this direction several types of vegetables and fruits have been recognized and re-evaluated as beneficial phytochemical sources for flavonoids and polyphenolic components [44]. The usage of these bioactive plant compounds may have preventive potential for several chronic complications including cancer [45].

It is widely recognized that the disruption of the ovulation process can be identified through measurement of the reproductive hormones [46]. Previous research has shown that a range of environmental toxicants can negatively impact female reproduction by affecting different reproductive tissues and functions [47]. Our existing work found that AOM injection resulted in an elevation of the levels of reproductive hormones. These change could be due to the occurrence of structural abnormalities and changes in the hypothalamic-pituitary axis function, resulting in the secretion of LH and FSH in a more direct manner by modifying the feedback of

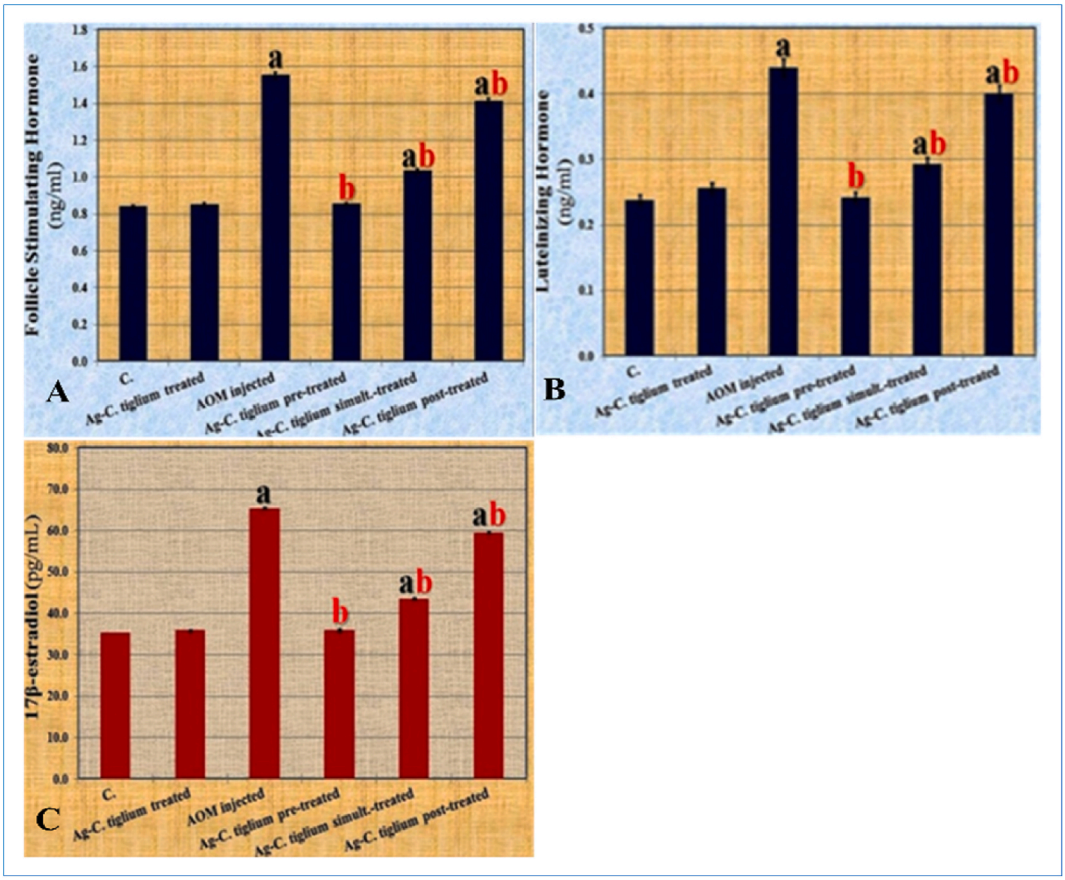

Fig. 12. Impact of Silver *C. tiglium* nano-extract and with/without Azoxymethane on reproductive related hormone. **A)** follicle stimulating hormone (FSH), **B)** luteinizing hormone (LH) and **C)** 17β-estradiol (E2) in sera of rats. Data were expressed as mean ± SE (of five replicates), **a**: significant difference from control group, **b**: significant difference from toxic (AOM injected) group at ($P \leq 0.05$).

these hormones [48]. It is possible that the action of steroid hormones, whether mimicking or antagonizing, could alter the glycosylation of LH and FSH, thereby reducing their biological activity. Additionally, the elevation of FSH and LH levels may be related to the induction of internucleosomal fragmentation and subsequent inactivation of enzymes involved in follicular cells, as well as a decrease in the number of LH receptors in atretic follicles, or dramatic changes in the overall structure of the ovary in response to exposure to these toxicants, leading to an accumulation of FSH and LH [49].

Furthermore, the increase in FSH and LH levels may be due to the enhancement of gonadotropin-releasing hormone expression in the hypothalamic preoptic area, which stimulates the secretion of these hormones [50]. As a result, the accumulated FSH stimulates ovarian follicles to undergo apoptosis, leading to ovarian failure [51]. The gonadal organs under the impact of FSH and LH mainly produce E2. The rise in the concentration of these hormones is recognizable to have a positive feedback effect on the activity of the pituitary gland, where they regulate the gonadotropin secretions [52]. The present work suggests that; higher concentration of the E2 hormone in the blood of the AOM-injected rats could be linked to an upregulation of the aromatase enzyme, which converts testosterone into estradiol in primary rat granulosa cells. Additionally, it may also disrupt steroidogenesis in swine granulosa cells [53].

The silver *C. tiglium* nano-extract reduced the hormonal levels of the all treated rat groups compared to with the AOM-injected group. This may be due to the presence of phenolic compounds that were elevated in conjunction with incorporating Ag-NPs as reported by Shousha et al. [54] and Aboulthana et al. [31]. The phenolic compounds had a positive effect on the gonads by regulating the secretion of these hormones into the circulation of female rats. Additionally, the hypothalamus and the anterior pituitary may be obviously impacted by these compounds, as the secretion of FSH and LH is regulated by the gonadotropin releasing-hormone secreted from the hypothalamus [41]. Our study also suggests that phenolic compounds may improve *in vivo* folliculogenesis and provide evidence for ovarian protection. The mechanisms underlying these effects could be through increasing granulosa cell proliferation, E2 and FSH secretion, which may be related to their antioxidant properties as reported by Chattopadhyay et al. [55].

Protein is highly susceptible to oxidation, particularly depending on the amount of oxidation-sensitive amino acid residues that it contain [56]. The electrophoretic technique is utilized to separate, identify, and quantify various proteins and isoenzymes based on the shape, size, and net charge of each molecule. Therefore, it is utilized for analysis of the stoichiometry of a particular subunit within a complex protein. Each band consists of a set of proteins with distinct metabolic properties [57].

Electrophoretic analysis can detect alterations at a qualitative scale by obscuring one or more naturalistic bands in addition to the presence of abnormal bands. The quantitative alterations alternatively might occur by changing the quantity of bands detected at normal mobility. The SI value is solely associated with the tissue's physiological condition. Low values of SI% are typically accompanied by changes in the arrangement and number of electrophoretically separated bands [58]. In the current study, this technique was utilized to demonstrate the adverse effect of AOM on the intracellular macromolecules within the ovarian and uterine tissues of rats.

The existing research found that AOM treatment led to physiological changes in the electrophoretic pattern of proteins in ovarian and uterine tissues. This could be due to the influence of 1,2-Dimethylhydrazine, which is mainly metabolized by cytochrome P450 2E1 (CYP2E1) into electrophilic metabolites. These metabolites may impact neoplastic processes by suppressing and destroying intercellular contacts, causing a loss of apical-basal polarity in the epithelium, and reducing adhesion to the basal membrane. These changes can lead to alterations in the cell phenotype or its dedifferentiation. As a result, this leads to a decrease in the expression of the proteins involved in the formation of intercellular contacts [59]. Likewise, Aboulthana et al. [60] suggested that changes in electrophoretic mobility could be due to the impact of free radicals on the integrity of the polypeptide chain within the protein molecule. This could result in sulfhydryl-mediated cross linking of labile amino acids, leading to polypeptide chains fragmentation. In the same vein, Avery [61] stated that changes could involve the excessive reactive oxygen species (ROS) directly reacting with the functional groups of aromatic side chains, leading to the irreversible formation of carbonyl products during the oxidation process.

Lipoproteins carry a variety of lipids in varying proportions. The density of lipoproteins has a direct proportional relationship with the amount of protein they contain and an inverse proportional relationship with the amount of lipid they carry [62]. Therefore, the change in lipid component occurring in the pattern of native protein may indicate alterations in the protein portion [60]. Our study demonstrated that; the AOM treatment resulted in physiological alterations in the electrophoretic lipid moiety of protein patterns. This was due to the accumulation of products from CYP2E1-mediated oxidation, which occurred as a consequence of the exhaustion of antioxidant defenses. This led to an attack on the lipid portion, resulting in denaturation of the lipid moieties of proteins and oxidative modifications [63].

Calcium is considered a trace element possessing a prognostic significance in the incidence and progression of cancerous tumors [64]. The calcium moiety of native proteins is found in the cytoplasm of various cells and plays a role in cell cycle progression and differentiation [65]. It plays a crucial role in regulating cAMP cell signaling and activating photoreceptor guanylate cyclase. Mutations in this gene are associated with retinal dystrophy [66].

In the current research, it was noted that AOM injection led to physiological changes in the native electrophoretic pattern. This may be linked to the modulation of gene expression responsible for the synthesis of these proteins [67]. The intermediates produced during AOM metabolism create an overabundance of ROS that interact with DNA, forming DNA adducts. This leads to DNA mutations and directly impacts the synthesis of a wide variety of proteins [68].

Administration of silver nano-extract reduced the harmful effects caused by the presence of a wide range of active constituents (polyphenolic compounds) that raised due to the metal nanoparticles (M-NPs) into in various native protein patterns [31,58]. Nanoparticles have been found to reach and accumulate in female reproductive organs, such as the ovary and uterus. This accumulation has been linked to a reduction in the number of mature oocytes and interference with the growth of primary and secondary follicles upon entry of the nanoparticles [69]. In the present study, it was found that the nano-extract improved the native protein patterns necessary for regulating the cell cycle in healthy cells. This improvement was attributed to presence of Ag-NPs, which have the

capability to facilitate DNA replication, cell growth and division, and organism renewal [70].

Oxidative stress occurs when the production of ROS outweighs the body's capacity to neutralize them with antioxidants. This can significantly impact various reproductive functions, including ovarian steroidogenesis, corpus luteal activity, oocyte maturation, and luteolytic processes [71]. The activities of antioxidant enzymes vary from tissue to tissue, making them a tissue-dependent tool. The abnormalities induced by AOM in the electrophoretic patterns of POX and CAT isoenzyme may be related to the degeneration of their protein portions due to the overproduction of ROS. ROS can alter the immunological and physico-chemical properties of endogenous POX and CAT enzymes, leading to structural and functional abnormalities [72,73]. Furthermore, the changes in these electrophoretic isoenzymes could be attributed to AOM binding to the native macromolecules, resulting in modulation of the secondary structure of these enzymes [74]. The silver nanoparticles (Ag-NPs) obtained from plant extracts have demonstrated exceptional antioxidant properties and significantly elevated levels of antioxidant enzymes, which are associated with reducing the by-products of peroxidation reactions [75]. Additionally, they improved the electrophoretic patterns of CAT and POX isoenzymes through their interaction with nucleic acids, enhancing the synthesis, replication, and structural integrity of DNA and RNA [76].

The EST electrophoretically pattern was utilized to investigate the impact of various carcinogenic and non-carcinogenic chemicals. In the existed study it was observed that; AOM induced variations in this isoenzyme pattern consistent with the findings of Tyndall et al. [77], who noted alterations in the native isoenzyme pattern after 7 days of exposure to the chemicals. Moreover, Davidson et al. [78] also found that the electrophoretic EST pattern was qualitatively changed after exposure to a nitrogenous toxicant. The changes in these isoenzymes appeared to be a physiological changes dependable markers occurred in ovarian granulosa cells as a consequence of the oxidative stress, imbalances in sex hormones, inflammation, and apoptosis [79].

Electrophoretically, abnormalities in the α- and β-EST isoenzyme patterns may indicate an increase in oxidative stress and the production of ROS. This can lead to alterations in the structure and function of albumin [80,81]. Additionally, the alterations in the EST pattern could be due to differences in glycosylation of EST types, resulting in modifications to the glycosylated EST forms. Abnormal glycosylation can increase the likelihood of protein degradation and impact the stability of EST. Furthermore, these alterations may be linked to an elevation in the quantity of ligand binding sites on receptor proteins and the concentration of unoccupied binding sites of estrogenic receptors in the reproductive organs of AOM-injected rats [82].

The silver nano-extract improved the electrophoretic isoenzyme patterns by increasing the active phyto-constituents after incorporating Ag-NPs. This helped maintain the antioxidant state of tissue and the bio-macromolecules integrity. Furthermore, capped Ag-NPs biosynthesized using plant extract through green nanotechnology exhibited higher antioxidant properties compared to uncapped Ag-NPs [83].

The pathological study in our research was conducted to clarify the toxic and carcinogenic effects of the hydrazine derivative AOM. The histopathological findings showed that the control and silver *C. tiglium* nano-treated rats exhibited normal growing follicles and normal endometrial mucosa, indicating the safety and tissue nontoxicity of nano silver *C. tiglium* extract. The rats treated with both silver *C. tiglium* nano + AOM, either in the pre-treated group or the post-treated group, displayed mild ovarian and endometrial degenerative changes. On the other hand, the rats treated with silver *C. tiglium* nano-extract simultaneously with AOM injection exhibited severe ovarian granulosa cell degeneration and necrosis, accompanied by endometrial epithelial metaplastic changes transforming from simple columnar to stratified columnar epithelium. The AOM-treated rats exhibited severe lutein cell degeneration and coagulative necrosis.

The uterus of this group showed a case of an endometriotic cyst abnormally embedded in the myometrium containing uterine glandular tissue. These histopathological findings especially in both the simulated silver *C. tiglium* nano extract + AOM group and the AOM positive control group could be attributed to the toxic and carcinogenic effect of AOM. This effect is clarified in several literatures reports, including Alabdullah et al. [84] Kurus et al. [14].

It is well established that the hydrazine derivatives DMH and its metabolite AOM toxicity lead to the formation of a high level of toxic free radicals, which in turn causes adipose tissue saponification and cellular protein denaturation. This leads to several tissue changes such as cellular vacuolar degeneration and necrosis, as well as hemorrhage and infiltration of inflammatory cells [85]

DMH is considered a potent carcinogenic agent that causes oxidative stress, tissue damage, and DNA mutation. Firstly, DMH is oxidized to AOM and then hydroxylated in the liver by the cytochrome P450-dependent pathway to form methylazoxymethanol (MAM). MAM translocates to the intestinal lumen through bile juice and circulation. MAM is thermolabile at body temperature, where it spontaneously decomposes to form the alkylating agent methyldiazonium ion, which in turn produces a carbonium reactive ion capable of alkylating macromolecules such as DNA, RNA, and proteins through non-enzymatic and enzymatic processes in colonic tissue. The alkylation of oxygen atoms in the nitrogenous bases increases the likelihood of DNA mispairing. Alkylated guanine can pair with thymidine instead of cytosine by donating a proton, leading to base modifications. This can result in mispairing of guanine with thymine and cytosine with adenine during subsequent replication, strongly suggesting mutagenesis and carcinogenesis [8,10].

The molecular mechanisms implicit in malignant endometriosis transformation are still unclear, but the imbalance in redox homeostasis may be implicated. The endometriotic cysts contain high levels of iron, and endometriotic cells can survive in the presence of a highly reactive oxygen species (ROS) environment. Haemoglobin, iron, and heme derivatives lead to DNA damage and mutations that promote the survivability and proliferation of endometrial cells and also cause ectopic implantation. However, high iron levels can cause cell death as a result of dramatic oxidative stress [86,87].

In this study, we used the immunohistochemical protocol (IHC) in the ovary and uterus to confirm the carcinogenic effect of the hydrazine derivative AOM by detecting cytokeratin 7 (CK-7) as an ovarian and endometrial tumor marker. This trend is come in accordance with Kriplani and Patel [88], who reported a significant development in the utilization of the IHC protocol in the diagnosis of ovarian pathology. Ovarian tumors had distinctive IHC characteristics, and stains could be used to suggest or confirm a diagnosis. IHC is able to differentiate between ovarian metastatic carcinomas and primary carcinomas, especially those of colorectal origin.

Cytokeratins (CKs) are a wide subgroup of the cellular intermediate filament (IF) proteins, fundamentally expressed in the epithelial tissues and coded by keratin genes. CKs are characterized by resistant to degradation process, very antigenic, and exhibits a great fidelity of expression. All CKs share in the basic molecular structure of cytoplasmic IF proteins. Their expression is developmentally regulated and differentiation-dependent, and also they are specific for different epithelial types [89].

In our study, the immunohistochemical findings for the detection of the CK-7 tumor marker in ovarian and uterine tissues revealed that both the control group and the silver *C. tiglium* nano-extract rat group showed negative immunoreaction for the CK-7 marker. However, the silver *C. tiglium* nano-extract + AOM pre-treated group showed a mild positive immunoreaction. Variable results were recorded in both ovarian and uterine tissues of the silver *C. tiglium* nano-extract + AOM post-treated group. The ovaries illustrated negative immunoreaction, while the uterus showed intracytoplasmic moderate positive immunoreaction. In both the AOM-treated rats and the silver *C. tiglium* nano-extract simultaneous-treated + AOM-treated group, moderate positive immunoreaction was noticed adjacent to the corpus luteum and in the endometrial perivascular spaces.

The use of CK-7 and its IHC findings in our study could be clarified as follows: Cytokeratins (CKs) are structural cellular cytoskeletal proteins that exist in epithelial cells and tumors originating from epithelial cells. Neoplastic cells commonly maintain CK marker expression, making specific anti-CK antibodies valuable in routine IHC diagnosis for defining tumor origins, especially in metastases. CK-7 is found in several glandular and ductal epithelia, including the ovary, endometrium, lung, mammary glands, pancreas, skin, and salivary gland. Expression of CK-7 is predominantly observed in cases of adenocarcinomas, except for those originating from the colon and prostate, kidney, and skin [25].

CK-7 marker is of molecular weight 54 kDa and naturally alkaline. It is expressed in several types of adenocarcinoma. Researches have proven that CK-7 is a positive provider for malignant neoplasm progression, and its malignancy expression is greater than that in naturalistic tissues [26]. The change in CK expression concentration could be change the cellular cytoskeletal components synthesis and or the cell deformation capability that elevates risk of the basement membrane breaking during the early neoplastic cells development, led to elevation of the depth of cancer cell infiltrations into the underling tissue. CK-7 can stimulate the forming of local pseudopodia and enhance the cancer cells proliferation rate, so that the CK-7 overexpression accelerate the cancer cells metastasis, vascular invasion, myometrial invasion, and lymph node metastasis therefore the CK-7 protein overexpression accompanied with the grade of disease deterioration [90].

Furthermore, in this research work; *C. tiglium* seeds extract complexed with silver nanoparticles as a trial for clarifying its natural anticancer protectant effect and competing the toxic and carcinogenic effects of the AOM metabolite, that due to several literature which contributed the following knowledge. The uncontrolled mitotic division and the fast migration of cancer cells are the main cancer hallmarks. Thus, targeting to inhibit the cell proliferation or enhancing the apoptosis can contribute a ways for cancer treatment [91].

Indeed, *C. tiglium* extract is controversial in ~~research of~~ cancer treatment. *Croton* diterpenoids and alkaloids have been found to inhibit cell proliferation or promote programmed cell death (apoptosis) to control ~~of the~~ malignant cell growth. *C. tiglium* extract, at a suitable concentrations induce cellular apoptosis by increasing the expression of the Bax gene and declining the expression of the Bcl-2 gene [92,93]. The elevation of the Bax/Bcl-2 ratio can lead to a decrease in mitochondrial membrane potential, which is considered an early event in tumor cell apoptosis, resulting in the release of cytochrome *c* into the cytosol. This release then activates caspase-9, which in turn activates caspase-3. Consequently the caspase cascade was activated and Poly (ADP-ribose) polymerase (PARP) is cleaved leading to apoptosis [94].

The effect of silver nanoparticles complexed with *Crotonis Fructus* extracts on AOM-induced colon cancer in rats was evaluated to enhance its antioxidant efficiency. The experimental findings of this study illustrated that the level of inflammatory markers (MPO and C-RP) and colon tumor markers (CA19.9 and CEA) decreased when compared to rats treated with AOM only. Additionally, the nano-formulated *Crotonis Fructus* extracts significantly restored the kidney function to normal levels in rats [31].

5. Conclusion

Hydrazine poses an actual threat to the environment as well as causes many harmful effects on human and animal health via reaching the food chain. AOM as metabolites of hydrazine cause toxic and carcinogenic effects in reproductive organs as; metaplastic myometrial endometriotic cysts and endometrial metaplasia. This effect was confirmed immunohistochemically by detecting the CK-7 tumor marker in ovarian and uterine tissues of the AOM, simultaneous, and post-treated groups. Also, AOM leads to impairments in the electrophoretic protein and isoenzyme patterns in addition to impairment in the reproductive hormones FSH, LH, and estradiol E2. The *C. tiglium* seeds extract complexed with silver nanoparticles succeeded in ameliorating that where; CK-7 is slightly expressed in the pre-treated group. Moreover, silver *C. tiglium* nano extract relieved the negative effects on the tested reproductive hormones.

Abbreviation List

Abbreviations	Full terms
μm	Micro-meter
ADP	Adenosine Di Phosphate
$AgNO_3$	Silver Nitrate
AgNPs	Silver nanoparticles
ANOVA	Analysis of variance test
AOM	Azoxymethane

(*continued on next page*)

(*continued*)

B%	Band percent
B.W.	Body weight
BAX	Bcl-2-associated X protein
Bcl-2	B-cell lymphoma 2
BSA	Bovine Serum Albumin
C. tiglium	*Croton tiglium*
CA19.9	Carbohydrate Antigen 19.9
cAMP	Cyclic Adenosine Mono Phosphate
caspase	Cysteine-dependent, aspartate-specific peptidase
CAT	Catalase
CBB	Coomassie Brilliant Blue stain
CEA	Cancer Embryonic Antigen
CK-7	Cytokeratin 7
CKs	Cytokeratins
CRFTM	Cybersecurity Regulatory Framework Technology Management
CRP	C-reactive protein
CYP2E1	Cytochrome P450 2E1
DAB	Di Amino Benzidine stain
DMH	Dimethylhydrazines
E2	17β-estradiol hormone
EAOC	Endometriosis Accompanied by Ovarian Carcinoma
EG	Ethylene Glycol
ELISA	Enzyme-Linked Immuno-Sorbent Assay
EST	Esterase
FSH	Follicle Stimulating Hormone
g	Gram
GD	Genetic Distance
GIT	Gastro-Intestinal-Tract
H&E	Hematoxylin and eosin stain
HRP	Horse Radish Peroxidase
i.p.	Intraperitoneally
IF	Intermediate filament
IgG	Immuno-globulin-gamma
IHC	Immunohistochemistry
kDa	Kilo Dalton
LD_{50}	lethal dose 50 %
LH	Luteinizing Hormone
MAM	Methylazoxymethanol
mg/Kg BW	Milligram/Kilogram Body Weight
mL	Mille-litre
mM	Milli-mole
MN	Micronuclei
$MnCl_2$	Manganese Chloride
M-NPs	Metal nanoparticles
MPO	Myeloperoxidase
n	Number
N_2H_4	Hydrazine
NBF	Neutral Buffered Formalin
ng/mL	Nano gram/millilitre
PAGE	Polyacrylamide Gel Electrophoresis
PARP	Poly-ADP ribose polymerase
PBS	Phosphate buffer saline
pg/mL	Pico gram/millilitre
POX	Peroxidase
PSI	Pounds per Square Inch
PVP	Polyvinylpyrrolidone
Qty	Quantity
Rfs	Relative factor electrophoresis
ROS	Reactive oxygen species
rpm	Revolution per minute
SBB	Sudan Black B stain
SE	Standard error
SI	similarity index
SPSS	Statistical Package for Social Sciences
Tris/EDTA	Tris-ethylene-di-amine tetra-acetic acid

Ethics approval

The Animal Ethics Committee of the National Research Centre, Dokki, Giza, Egypt approved all experiments with approval number

(16116).

Consent for publication

All authors review and approve the manuscript for publication.

Funding and acknowledgment

Not applicable.

Data availability

The authors confirm that the data supporting the findings of this study are available from the corresponding author; Mohamed Seif.

CRediT authorship contribution statement

Wael Mahmoud Aboulthana: Writing – original draft, Data curation, Conceptualization. **Abd El-Nasser A. Madboli:** Writing – original draft, Investigation, Data curation. **Amal Gouda Hussien:** Investigation, Data curation. **Mohamed Seif:** Writing – review & editing, Validation, Investigation, Data curation, Conceptualization.

Declaration of competing interest

The authors declare that they have no known competing financial interests or personal relationships that could have appeared to influence the work reported in this paper.

Appendix A. Supplementary data

Supplementary data to this article can be found online at https://doi.org/10.1016/j.heliyon.2024.e38820.

References

[1] R.A. Canady, J.E. Hanley, A.S.J.R.a. Susten, ATSDR science panel on the bioavailability of mercury in soils: lessons learned 17 (1997) 527–532.
[2] E.K. Al-Hamdany, K.H. Al-Mallah, H.K.J.I.J.o.V.S. Ismail, Histopathological evaluation of lesions induced by dimethyl hydrazine in male rats 36 (2022) 115–121.
[3] B. Aigner, U. Darsow, M. Grosber, J. Ring, S.J.D. Plötz, Multiple Basal Cell Carcinomas after Long-Term Exposure to Hydrazine: Case Report and Review of the Literature, vol. 221, 2010, pp. 300–302.
[4] P.S. Spencer, G.E.J.C.R.i.T. Kisby, Role of Hydrazine-Related Chemicals in Cancer and Neurodegenerative Disease, vol. 34, 2021, pp. 1953–1969.
[5] S. Sridhar, G. Susheela, G.J. Reddy, A.A.J.P.I. Khan, Crosslinked Chitosan Membranes: Characterization and Study of Dimethylhydrazine Dehydration by Pervaporation, vol. 50, 2001, pp. 1156–1161.
[6] O.O. Hamiza, M.U. Rehman, M. Tahir, R. Khan, A.Q. Khan, A. Lateef, F. Ali, S.J.A.P.J.o.C.P. Sultana, Amelioration of 1, 2 Dimethylhydrazine (DMH) Induced Colon Oxidative Stress, Inflammation and Tumor Promotion Response by Tannic Acid in Wistar Rats, vol. 13, 2012, pp. 4393–4402.
[7] S. Walia, R. Kamal, D. Dhawan, S.J.D.d. Kanwar, sciences, Chemoprevention by probiotics during 1, 2-dimethylhydrazine-induced colon carcinogenesis in rats 63 (2018) 900–909.
[8] S. Shebbo, M. El Joumaa, R. Kawach, J.J.H. Borjac, Hepatoprotective Effect of Matricaria Chamomilla Aqueous Extract against 1, 2-Dimethylhydrazine-Induced Carcinogenic Hepatic Damage in Mice, vol. 6, 2020.
[9] U. Umeaku, D.A. Ofusori, O.P. Umeaku, T.A.J.I.J.o.H.A. Edward, The effect of aqueous extract of Ocimum gratissium (Linn) on 1, 2-dimethyl hydrazine induced colon cancer in male Wistar rats 2 (2020) 22–35.
[10] K. Venkatachalam, R. Vinayagam, M. Arokia Vijaya Anand, N.M. Isa, R.J.T.r. Ponnaiyan, Biochemical and molecular aspects of 1, 2-dimethylhydrazine (DMH)-induced colon carcinogenesis, a review 9 (2020) 2–18.
[11] W. Li, M. Zhou, N. Xu, Y. Hu, C. Wang, D. Li, L. Liu, D.J.B. Li, Comparative analysis of protective effects of curcumin, curcumin-β-cyclodextrin nanoparticle and nanoliposomal curcumin on unsymmetrical dimethyl hydrazine poisoning in mice 7 (2016) 334–341.
[12] B.S. Reddy, Animal Models for Colon Cancer Chemoprevention, 2002.
[13] A. Bhatia, Y.J.A. Kumar, Cancer Cell Micronucleus: an Update on Clinical and Diagnostic Applications, vol. 121, 2013, pp. 569–581.
[14] M. Kurus, A. Bay Karabulut, E. Taslidere, O.J.A. Otlu, Preventive effects of Resveratrol against azoxymethane-induced testis injury in rats 49 (2017) e12674.
[15] R.H.J.A.i.a.p. Young, From krukenberg to today: the ever present problems posed by metastatic tumors in the ovary: part I, Historical perspective, general principles, mucinous tumors including the krukenberg tumor 13 (2006) 205–227.
[16] W.G. McCluggage, R.H.J.T.A.j.o.s.p. Young, Primary ovarian mucinous tumors with signet ring cells: report of 3 cases with discussion of so-called primary Krukenberg tumor 32 (2008) 1373–1379.
[17] S. Lam Shang Leen, N.J.J.o.c.p. Singh, Pathology of Primary and Metastatic Mucinous Ovarian Neoplasms, vol. 65, 2012, pp. 593–597.
[18] B. Rekhi, S. George, B. Madur, R. Chinoy, R. Dikshit, A.J.D.P. Maheshwari, Clinicopathological Features and the Value of Differential Cytokeratin 7 and 20 Expression in Resolving Diagnostic Dilemmas of Ovarian Involvement by Colorectal Adenocarcinoma and Vice-Versa, vol. 3, 2008, pp. 1–7.
[19] M.R.A. Hussein, A.S. Alqahtani, A.F. Ibrahim, M.F. Bazeed, S.A. Alqahtani, A.M. Alasmari, A.M. Homran, S.A. Assiri, T.M.R.A. Hussein, E.E.J.I.J.C.E.M. Abu-Dief, Case Report Ovarian Metastasis from Adenocarcinoma of the Rectosigmoid Colon, vol. 16, 2023, pp. 155–165.
[20] D. Standing, E. Feess, S. Kodiyalam, M. Kuehn, Z. Hamel, J. Johnson, S.M. Thomas, S.J.C. Anant, The Role of STATs in Ovarian Cancer: Exploring Their Potential for Therapy, vol. 15, 2023, p. 2485.
[21] H. Machida, K. Matsuo, W. Yamagami, Y. Ebina, Y. Kobayashi, T. Tabata, M. Kanauchi, S. Nagase, T. Enomoto, M.J.G.o. Mikami, Trends and Characteristics of Epithelial Ovarian Cancer in Japan between 2002 and 2015: A JSGO–JSOG Joint Study, vol. 153, 2019, pp. 589–596.

[22] F.J.C. Guidozzi, Endometriosis-associated Cancer, vol. 24, 2021, pp. 587–592.
[23] D.W. Agnew, N.J.J.T.i.d.a. MacLachlan, Tumors of the Genital Systems, 2016, pp. 689–722.
[24] W. Hananeh, Z. Ismail, M. Daradka, Tumors of the reproductive tract of sheep and goats: a review of the current literature and a report of vaginal fibroma in an Awassi Ewe, Vet. World 12 (6) (2019) 778–782 (Abstract).
[25] J. Hrudka, H. Fišerová, K. Jelínková, R. Matěj, P.J.S.R. Waldauf, Cytokeratin 7 expression as a predictor of an unfavorable prognosis in colorectal carcinoma 11 (2021) 17863.
[26] Y. Wu, M. Lv, T. Qian, Y.J.A.o.P.M. Shen, Correlation analysis of Ki67 and CK7 expression with clinical characteristics and prognosis of postoperative cervical adenocarcinoma patients 10 (2021) 9544552–9549552.
[27] J. Al-Maghrabi, E. Emam, W.J.S.J.o.G.O.J.o.t.S.G.A. Gomaa, Immunohistochemical Staining of Cytokeratin 20 and Cytokeratin 7 in Colorectal Carcinomas: Four Different Immunostaining Profiles, vol. 24, 2018, p. 129.
[28] T. Zhang, Z. Liu, X. Sun, Z. Liu, L. Zhang, Q. Zhang, W. Peng, C.J.J.o.P. Wu, Pharmacology, Botany, traditional uses, phytochemistry, pharmacological and toxicological effects of Croton tiglium Linn, a comprehensive review 74 (2022) 1061–1084.
[29] M. Balzarro, E. Rubilotta, N. Trabacchin, A. Soldano, C. Cerrato, F. Migliorini, V. Mancini, A.L. Pastore, A. Carbone, L.J.J.o.C.M. Cormio, Early and Late Efficacy on Wound Healing of Silver Nanoparticle Gel in Males after Circumcision, vol. 9, 2020, p. 1822.
[30] I.K. Siakavella, F. Lamari, D. Papoulis, M. Orkoula, P. Gkolfi, M. Lykouras, K. Avgoustakis, S.J.P. Hatziantoniou, Effect of Plant Extracts on the Characteristics of Silver Nanoparticles for Topical Application, vol. 12, 2020, p. 1244.
[31] W.M. Aboulthana, A.M. Youssef, A.M. El-Feky, N. Ibrahim, M.M. Seif, A.K.J.E.J.C. Hassan, Evaluation of Antioxidant Efficiency of Croton Tiglium L. Seeds Extracts after Incorporating Silver Nanoparticles, vol. 62, 2019, pp. 181–200.
[32] N. Sunagawa, M. Inamine, T. Morioka, I. Chiba, N. Morita, Y. Aoki, M. Suzui, N.J.M.M.R. Yoshimi, Inhibitory Effect of Rice Bran-Derived Crude Glycosphingolipid on Colon Preneoplastic Biomarker Lesions Induced by Azoxymethane in Male F344 Rats, vol. 2, 2009, pp. 45–49.
[33] D.M.J.C.p.i.t. Creasy, Histopathology of the Male Reproductive System I: Techniques, vol. 12, 2002, p. 16, 13. 11-16.13. 18.
[34] K.H. Kim, C.W.J.N.m. Roberts, Targeting EZH2 in Cancer, vol. 22, 2016, pp. 128–134.
[35] M.M.J.A.b. Bradford, A rapid and sensitive method for the quantitation of microgram quantities of protein utilizing the principle of protein-dye binding 72 (1976) 248–254.
[36] O.M. Darwesh, H. Moawad, O.S. Barakat, W.J.R.J.o.P. El-Rahim, Biological, and Sciences, C, in: Bioremediation of Textile Reactive Blue Azo Dye Residues Using Nanobiotechnology Approaches, vol. 6, 2015, pp. 1202–1211.
[37] H.N. Subramaniam, K.A.J.J.o.b. Chaubal, b. methods, Evaluation of Intracellular Lipids by Standardized Staining with a Sudan Black B Fraction, vol. 21, 1990, pp. 9–16.
[38] S.A. Abd Elhalim, H.M. Sharada, I. Abulyazid, W.M. Aboulthana, S.T.J.J.o.A.P.S. Abd Elhalim, Ameliorative Effect of Carob Pods Extract (Ceratonia Siliqua L.) against Cyclophosphamide Induced Alterations in Bone Marrow and Spleen of Rats, vol. 7, 2017, pp. 168–181.
[39] M.J. Siciliano, C.R. Shaw, Separation and visualization of enzymes on gels, in: Zone Electrophoresis, Elsevier, 1976, pp. 185–209.
[40] A. Rescigno, E. Sanjust, L. Montanari, F. Sollai, G. Soddu, A. Rinaldi, S. Oliva, A.J.A.l. Rinaldi, Detection of laccase, peroxidase, and polyphenol oxidase on a single polyacrylamide gel, electrophoresis 30 (1997) 2211–2220.
[41] A. Ahmad, V. Maheshwari, A. Ahmad, R. Saleem, R.J.M.J.M.S. Ahmad, Observation of esterase-like-albumin activity during N'-Nitrosodimethylamine induced hepatic fibrosis in a mammalian model 5 (2012) 55–61.
[42] W. Ratcliffe, G. Carter, M. Dowsett, S. Hillier, J. Middle, M.J.A.o.c.b. Reed, Oestradiol Assays: Applications and Guidelines for the Provision of a Clinical Biochemistry Service, vol. 25, 1988, pp. 466–483.
[43] M. Nei, W.-H.J.P.o.t.N.A.o.S. Li, Mathematical Model for Studying Genetic Variation in Terms of Restriction Endonucleases, vol. 76, 1979, pp. 5269–5273.
[44] A. Albini, F. Tosetti, V.W. Li, D.M. Noonan, W.W.J.N.r.C.o. Li, Cancer Prevention by Targeting Angiogenesis, vol. 9, 2012, pp. 498–509.
[45] N.N. Mutyal, A. Radosevich, A.K. Tiwari, Y. Stypula, R. Wali, D. Kunte, H.K. Roy, V.J.P.o. Backman, Biological mechanisms underlying structural changes induced by colorectal field carcinogenesis measured with low-coherence enhanced backscattering, LEBS) spectroscopy 8 (2013) e57206.
[46] H. Snick, T. Snick, J. Evers, J.J.H.r. Collins, The Spontaneous Pregnancy Prognosis in Untreated Subfertile Couples: the Walcheren Primary Care Study, vol. 12, 1997, pp. 1582–1588.
[47] S. Rattan, C. Zhou, C. Chiang, S. Mahalingam, E. Brehm, J.A.J.J.o.E. Flaws, Exposure to endocrine disruptors during adulthood: consequences for female fertility 233 (2017) R109–R129.
[48] S. Patel, C. Zhou, S. Rattan, J.A.J.B.o.r. Flaws, Effects of endocrine-disrupting chemicals on the ovary 93 (20) (2015) 21–29.
[49] Y.-K. Lee, H.-H. Chang, W.-R. Kim, J. Kyu Kim, Y.-D.J.A.z.h.r.i.t. Yoon, Effects of Gamma-Radiation on Ovarian Follicles, vol. 49, 1998, pp. 147–153.
[50] C. Roth, M. Lakomek, H. Schmidberger, H.J.K.P. Jarry, Cranial Irradiation Induces Premature Activation of the Gonadotropin-Releasing-Hormone, vol. 213, 2001, pp. 239–243.
[51] K. Yacobi, A. Wojtowicz, A. Tsafriri, A.J.E. Gross, Gonadotropins Enhance Caspase-3 And-7 Activity and Apoptosis in the Theca-Interstitial Cells of Rat Preovulatory Follicles in Culture, vol. 145, 2004, pp. 1943–1951.
[52] H. Shivalingappa, N. Satyanarayan, M. Purohit, A. Sharanabasappa, S.J.J.o.e. Patil, Effect of Ethanol Extract of Rivea Hypocrateriformis on the Estrous Cycle of the Rat, vol. 82, 2002, pp. 11–17.
[53] G. Basini, F. Bianchi, S. Bussolati, L. Baioni, R. Ramoni, S. Grolli, V. Conti, F. Bianchi, F.J.E. Grasselli, e. safety, Atrazine Disrupts Steroidogenesis, VEGF and NO Production in Swine Granulosa Cells, vol. 85, 2012, pp. 59–63.
[54] W.G. Shousha, W.M. Aboulthana, A.H. Salama, M.H. Saleh, E.A.J.B.o.t.N.R.C. Essawy, Evaluation of the biological activity of Moringa oleifera leaves extract after incorporating silver nanoparticles, Vitro study 43 (2019) 1–13.
[55] S. Chattopadhyay, S. Pal, D. Ghosh, J.J.T.S. Debnath, Effect of Dietary Co-administration of Sodium Selenite on Sodium Arsenite-Induced Ovarian and Uterine Disorders in Mature Albino Rats, vol. 75, 2003, pp. 412–422.
[56] I. Abulyazid, M. Abdalla, H. Sharada, M. Abd El Kader, W.J.I.J.o.R.S.R. Kamel, Protective Effect of Salicin Isolated from Egyptian Willow Leaves (Salix Subserrata) against Gamma-Radiation-Induced Electrophoretic and Molecular Changes in Epididymal Tissue in Rats, vol. 6, 2015, pp. 4421–4435.
[57] P. Shah, P. Bhatt, P. Patel, V. Ghori, P.J.I.J.P.H.S. Vaghela, Study of Electrophoretic Pattern in Serum of Multiple Myeloma Patients, vol. 1, 2010, pp. 116–131.
[58] W.M. Aboulthana, N.I. Omar, A.M. El-Feky, E.A. Hasan, N.E.-S. Ibrahim, A.M.J.A.P.J.o.C.P.A. Youssef, In vitro study on effect of zinc oxide nanoparticles on the biological activities of croton Tiglium L, Seeds extracts 23 (2022) 2671.
[59] V. Bekusova, L. Droessler, S. Amasheh, A.G.J.I.J.o.M.S. Markov, Effects of 1, 2-dimethylhydrazine on Barrier Properties of Rat Large Intestine and IPEC-J2 Cells, vol. 22, 2021 10278.
[60] W.M. Aboulthana, M. Ismael, H.S.J.I.J.C.P.R.R. Farghaly, Assessment of Mutagenicity Induced by Toxic Factors Affecting Ovarian Tissue in Rats by Electrophoresis and Molecular Dynamic Modeling, vol. 7, 2016, pp. 347–359.
[61] S.V.J.B.J. Avery, Molecular Targets of Oxidative Stress, vol. 434, 2011, pp. 201–210.
[62] K.M. Bass, C.J. Newschaffer, M.J. Klag, T.L.J.A.o.i.m. Bush, Plasma lipoprotein levels as predictors of cardiovascular death in women 153 (1993) 2209–2216.
[63] A.E.-K.B. El-Sayed, W.M. Aboulthana, A.M. El-Feky, N.E. Ibrahim, M.M.J.M.b.r. Seif, Bio and Phyto-Chemical Effect of Amphora Coffeaeformis Extract against Hepatic Injury Induced by Paracetamol in Rats, vol. 45, 2018, pp. 2007–2023.
[64] E. Altekin, C. Çoker, A.R. Şişman, B. Önvural, F. Kuralay, Ö.J.J.o.T.E.i.M. Kırımlı, Biology, The Relationship between Trace Elements and Cardiac Markers in Acute Coronary Syndromes, vol. 18, 2005, pp. 235–242.
[65] L.J.T.A.j.o.p. Mazzucchelli, Protein S100A4: Too Long Overlooked by Pathologists?, vol. 160, 2002, pp. 7–13.
[66] A.M. Payne, S.M. Downes, D.A. Bessant, C. Plant, T. Moore, A.C. Bird, S.S.J.J.o.m.g. Bhattacharya, Genetic analysis of the guanylate cyclase activator 1B (GUCA1B) gene in patients with autosomal dominant retinal dystrophies 36 (1999) 691–693.
[67] R.S. Ismail, R.L. Baldwin, J. Fang, D. Browning, B.Y. Karlan, J.C. Gasson, D.D.J.C.r. Chang, Differential gene expression between normal and tumor-derived ovarian epithelial cells 60 (2000) 6744–6749.

[68] D.W. Rosenberg, C. Giardina, T.J.C. Tanaka, Mouse Models for the Study of Colon Carcinogenesis, vol. 30, 2009, pp. 183–196.
[69] L. Dianová, F. Tirpák, M. Halo, T. Slanina, M. Massányi, R. Stawarz, G. Formicki, R. Madeddu, P.J.T. Massányi, Effects of Selected Metal Nanoparticles (Ag, ZnO, TiO2) on the Structure and Function of Reproductive Organs, vol. 10, 2022, p. 459.
[70] H.K. Matthews, C. Bertoli, R.A.J.N.R.M.C.B. de Bruin, Cell Cycle Control in Cancer, vol. 23, 2022, pp. 74–88.
[71] P. Newsholme, V.F. Cruzat, K.N. Keane, R. Carlessi, P.I.H.J.B.J. de Bittencourt Jr, Molecular Mechanisms of ROS Production and Oxidative Stress in Diabetes, vol. 473, 2016, pp. 4527–4550.
[72] T. Tian, Z. Wang, J.J.O.m. Zhang, c. longevity, Pathomechanisms of oxidative stress in inflammatory bowel disease and potential antioxidant therapies (2017) 2017.
[73] A.A.J.B.S.J. Jabbar, Gastroprotective and Immuno-Supportive Role of Alcea Kurdica against Stress Induced Lesion in Japanese Quails, vol. 19, 2022, p. 716, 0716.
[74] M. Mansouri, M. Pirouzi, M.R. Saberi, M. Ghaderabad, J.J.M. Chamani, Investigation on the Interaction between Cyclophosphamide and Lysozyme in the Presence of Three Different Kind of Cyclodextrins: Determination of the Binding Mechanism by Spectroscopic and Molecular Modeling Techniques, vol. 18, 2013, pp. 789–813.
[75] R. Mata, J.R. Nakkala, S.R.J.B.A. Sadras, Therapeutic Role of Biogenic Silver and Gold Nanoparticles against a DMH-Induced Colon Cancer Model, vol. 146, 2023 213279.
[76] A. Ribeiro, S. Anbu, E. Alegria, A. Fernandes, P. Baptista, R. Mendes, A. Matias, M. Mendes, M.G. da Silva, A.J.B. Pombeiro, Pharmacotherapy, Evaluation of Cell Toxicity and DNA and Protein Binding of Green Synthesized Silver Nanoparticles, vol. 101, 2018, pp. 137–144.
[77] C. Tyndall, H.B. Younghusband, A.J.J.o.V. Bellett, Some Adenovirus DNA Is Associated with the DNA of Permissive Cells during Productive or Restricted Growth, vol. 25, 1978, pp. 1–10.
[78] K.A. Davidson, R.L. Tyndall, N.K.J.C.-B.I. Clapp, Qualitative Alterations in Plasma Esterases in BALB/c Mice Following the Administration of Diethylnitrosamine, vol. 21, 1978, pp. 19–27.
[79] C. Caglayan, F.M. Kandemir, S. Yıldırım, S. Kucukler, M.A. Kılınc, Y.S.J.B. Saglam, Pharmacotherapy, Zingerone ameliorates cisplatin-induced ovarian and uterine toxicity via suppression of sex hormone imbalances, oxidative stress, inflammation and apoptosis in female wistar rats 102 (2018) 517–530.
[80] B. Gangadharan, R. Antrobus, R.A. Dwek, N.J.C.c. Zitzmann, Novel Serum Biomarker Candidates for Liver Fibrosis in Hepatitis C Patients, vol. 53, 2007, pp. 1792–1799.
[81] W.M. Aboulthana, W.G. Shousha, E.A.-R. Essawy, M.H. Saleh, A.H.J.A.P.J.o.C.P.A. Salama, Assessment of the Anti-cancer Efficiency of Silver Moringa Oleifera Leaves Nano-Extract against Colon Cancer Induced Chemically in Rats, vol. 22, 2021, p. 3267.
[82] O. Morozova, N.J.E.n.O. Kushlinskiĭ, Effect of 1, 2-dimethylhydrazine on the Level of Specific Binding and Ligand Affinity to the Estradiol Receptor in the Cytosol of Uterine Tissue in CBA Mice, vol. 9, 1987, pp. 54–56.
[83] A.K. Sidhu, N. Verma, P.J.F.i.N. Kaushal, Role of Biogenic Capping Agents in the Synthesis of Metallic Nanoparticles and Evaluation of Their Therapeutic Potential, vol. 3, 2022 801620.
[84] S.W. Alabdullah, S.A. Alsamir, I.A.J.E.J.B. AlRufaei, Effect of Thymoquinone on Some Biochemical and Hormonal Indices and Their Protective Effect on the Genital Organs of Rats after Cancer Induction in Laboratory, vol. 14, 2020, pp. 567–573.
[85] L. Ma, Y. Lang, X. Xin, W. Zhao, Q. Zhou, J. Wang, S.J.J.o.F.F. Dong, Polysaccharides extracted from hawthorn (Crataegus pinnatifida) exhibiting protective effects against DSS/AOM-induced colorectal, cancer in vivo 107 (2023) 105618.
[86] H.J.R.R. Kobayashi, Potential Scenarios Leading to Ovarian Cancer Arising from Endometriosis, vol. 21, 2016, pp. 119–126.
[87] H.J.E. Kobayashi, T. Medicine, Clinicopathological Characteristics, Molecular Features and Novel Diagnostic Strategies for the Detection of Malignant Transformation of Endometriosis, vol. 25, 2023, pp. 1–10.
[88] D. Kriplani, M.M.J.S.A.j.o.c. Patel, Immunohistochemistry: A Diagnostic Aid in Differentiating Primary Epithelial Ovarian Tumors and Tumors Metastatic to the Ovary, vol. 2, 2013, pp. 254–258.
[89] D. Vasilevska, V. Rudaitis, A. Adamiak-Godlewska, A. Semczuk-Sikora, D. Lewkowicz, D. Vasilevska, A.J.J.o.C. Semczuk, Cytokeratin Expression Pattern in Human Endometrial Carcinomas and Lymph Nodes Micrometastasis: a Mini-Review, vol. 13, 2022, p. 1713.
[90] B. Zhao, M.M. McDonald, M.B. Bhattacharjee, R.F. Barth, L.M.J.R.A.i.H.-. Buja, Cardiopulmonary Pathology in COVID-19, vol. 25, 2022, p. 1.
[91] P. Hainaut, A.J.C.o.i.o. Plymoth, Targeting the Hallmarks of Cancer: towards a Rational Approach to Next-Generation Cancer Therapy, vol. 25, 2013, pp. 50–51.
[92] P. Thien Thuong, N. Minh Khoi, S. Ohta, S. Shiota, H. Kanta, K. Takeuchi, F.J.A.-C.A.i.M.C. Ito, Ent-Kaurane Diterpenoids from Croton Tonkinensis Induce Apoptosis in Colorectal Cancer Cells through the Phosphorylation of JNK Mediated by Reactive Oxygen Species and Dual-Specificity JNK Kinase MKK4, vol. 14, 2014, pp. 1051–1061.
[93] C. Li, X. Wu, R. Sun, P. Zhao, F. Liu, C.J.A.P.J.o.C.P.A. Zhang, Croton Tiglium Extract Induces Apoptosis via Bax/Bcl-2 Pathways in Human Lung Cancer A549 Cells, vol. 17, 2016, p. 4893.
[94] Q.-l. Niu, H. Sun, C. Liu, J. Li, C.-x. Liang, R.-r. Zhang, F.-r. Ge, W.J.P.o. Liu, Croton Tiglium Essential Oil Compounds Have Anti-proliferative and Pro-apoptotic Effects in A549 Lung Cancer Cell Lines, vol. 15, 2020 e0231437.